

**ELECTROMAGNETIC FLOAT POLISHING
OF CERAMIC BALL BEARINGS**

by

MATTHEW L. DOCK

Bachelor of Science

Oklahoma State University

Stillwater, Oklahoma

1992

Submitted to the Faculty of the
Graduate College of the
Oklahoma State University
in partial fulfillment of
the requirements for
the Degree of
MASTER OF SCIENCE
May, 1995

**ELECTROMAGNETIC FLOAT POLISHING
OF CERAMIC BALLS FOR BEARING
APPLICATIONS**

Thesis Approved:



Thesis Adviser

Don A. Lucca





Dean of the Graduate College

SUMMARY

Advanced ceramics offer advantages over other materials in applications that require high stiffness, high temperature strength, high wear resistance, or high fatigue life. The ceramic ball bearing is a system that can operate in environments that would cause other bearings to fail. Unfortunately, ceramic bearing elements are expensive to manufacture and require reliability in performance in service.

Cost effective methods of ceramic element manufacturing are required to allow ceramic elements to be incorporated into mainstream manufacturing. Ultra-precision grinding machines can generate quality ceramic parts but this equipment can not handle spherical elements. For this reason, magnetic float polishing has been developed to lower the manufacturing cost, improve surface finish, and sphericity.

Magnetic float polishing was originated from the work done on magnetic fluid grinding in Japan. The process utilizes magnetic fluid, abrasive grains, and a drive spindle to polish the ceramic elements. The equipment utilized in magnetic fluid grinding and magnetic float polishing is similar to the equipment developed for magnetic abrasive finishing since the 1940's.

Magnetic float polishing is a technique that requires little capital expenditure, can be incorporated on existing machine tools, and can produce quality parts that withstand the mechanical and thermal stresses associated with the operation in advanced systems. The construction of magnetic float polishing apparatus has typically been with permanent

magnet systems. The electromagnetic apparatus developed here for the first time for finishing balls has promise of controlled magnetic field strength, stronger forces, and improved polishing efficiency.

An electromagnetic float polishing apparatus was designed and built to evaluate its performance in polishing and to compare it with the permanent magnet setup. ANSYS software was then used to improve on the initial electromagnetic design called straight field design. The modified design, now called a ring pole system, has shown the ability to polish ceramic ball bearing elements and improve on the sphericity of those parts. The equipment is capable of polishing small batches of 10-20 ceramic balls in a small polishing chamber allowing small batch production.

The electromagnetic polishing apparatus is capable of removing $6 \mu\text{m}/\text{min}$, allowing the apparatus to be utilized as a roughing station. During the rough polishing the average obtainable sphericity is approximately $3 \mu\text{m}$ obtained within 4 hours of starting the polishing process. The same equipment can then obtain a surface roughness, R_a , of 5 nm , allowing a single piece of equipment to transform a rough and out of shape ball into a smooth spherical element.

The ceramic ball elements have been characterized to determine the characteristics of the polishing apparatus, and the effects of polishing are categorized. High material removal rates and good sphericity control show the capabilities of the electromagnetic polishing apparatus and its application to future processing methods.

ACKNOWLEDGEMENTS

The author would like to express gratitude and thanks to Dr. Ranga Komanduri at Oklahoma State University for invaluable guidance and assistance during this research project. Working with him, and others in the research group, has been highly rewarding and pleasant experience that will be remembered for a lifetime.

This project has been funded in part by an ARPA contract on Ceramic Bearing Technology Program (F33615-92-5933) and a NSF grant (DDM9402895) on Design, Construction, and Optimization of Magnetic Fluid Assisted Polishing. The author likes to thank Dr. W. Coblenz of ARPA and K. R. Mecklenburg of WPAPB and Dr. K. Srinivasan and Dr. B.M. Kramer of NSF for their interest in this project. Special thanks to Dr. D.A. Lucca and Dr. C.E. Price for agreeing to serve on the thesis committee.

The original electromagnetic float polishing apparatus was developed by Dr. T. Shinmura of Utsunomia University with Professor R. Komanduri. The author thanks the contributions of Dr. T. Shinmura. The author also thanks Dr. N. Umehara, visiting assistant professor, from Tohoku University, Sandai, Japan, T.R. Ramamohan, M.R. Raghunandan, M. Fox, J. Hixon, S. Bhagavadula, and K. Mallika for their discussions and assistance through this investigation.

On a personal note, the author acknowledges the invaluable support and encouragement of his mother, family, and friends.

TABLE OF CONTENTS

LIST OF TABLES.....	viii
LIST OF FIGURES	ix
CHAPTER 1 INTRODUCTION	
1.1 Advantages of Advanced Ceramics.....	1
1.2 Conventional Production of Ceramic Components.....	2
1.3 New Finishing Techniques.....	3
1.4 Magnetic Float Polishing.....	7
CHAPTER 2 LITERATURE REVIEW	
2.1 Origin of Magnetic Field Assisted Polishing.....	10
2.2 Magnetic Fluid Grinding.....	11
2.3 Magnetic Float Polishing.....	13
2.4 Variables in Magnetic Float Polishing.....	14
2.5 Theoretical Considerations.....	20
CHAPTER 3 PROBLEM STATEMENT	
3.1 Advantages of Magnetic Float Polishing.....	22
3.2 Electromagnetic Float Polishing.....	24
CHAPTER 4 ANALYSIS AND INITIAL EVALUATION OF MAGNETIC FLOAT POLISHING APPARATUS	
4.1 Initial Design.....	25
4.2 Construction of Electromagnetic Polishing Apparatus.....	29
4.3 Initial Evaluation.....	33
4.4 ANSYS Analysis of Straight Field Electromagnetic Polishing Apparatus.....	35
4.5 ANSYS Analysis of Ring Pole Electromagnetic Apparatus.....	42
4.6 Experimental Evaluation of Forces in Straight Field and Ring Pole Designs.....	49
CHAPTER 5 DESIGN OF EXPERIMENTAL APPARATUS	
5.1 Evaluation of Polishing with Ring Pole Design.....	51
5.2 Convuluted Magnetic Field Intensifier.....	52
5.3 Design Modification for Removal of Excessive Heat.....	52

CHAPTER 6 TEST RESULTS

6.1	Experimental Procedure.....	54
6.2	Variables Involved in Electromagnetic Float Polishing.....	55
6.3	Electromagnetic Apparatus Polishing Results.....	56
6.4	Effect of Revolution Speed on Material Removal.....	57
6.5	Effect of Abrasive Grain type on Material Removal.....	58
6.6	Effect of Abrasive Size on Material Removal.....	58
6.7	Effect of Abrasive Grains on Surface Roughness.....	59
6.8	Control of Sphericity.....	60

CHAPTER 7 DISCUSSION

7.1	Construction of Electromagnetic Apparatus.....	64
7.2	Polishing Experiments.....	65

CHAPTER 8 CONCLUSIONS

8.1	Summary of Present Work.....	66
8.2	Recommendations for Future Work.....	67

BIBLIOGRAPHY.....	69
-------------------	----

APPENDIX A.....	71
-----------------	----

APPENDIX B.....	79
-----------------	----

APPENDIX C.....	88
-----------------	----

LIST OF TABLES

Table	Page
Table 1.1 Comparison of properties between silicon nitride and SUJ 2 bearing steel... 1	1
Table 2.1 Comparison between MFP with and without the addition of a float..... 14	14
Table 6.1 Attributes of ceramic balls for bearing applications..... 54	54
Table 6.2 Data for Cerbec ceramic ball..... 55	55
Table 6.3 Variables involved in electromagnetic float polishing..... 55	55
Table 6.4 Effect of abrasive type and size on final surface finish..... 60	60

LIST OF FIGURES

Figure		Page
Figure 1.1	Schematic of the magnetic abrasive finishing apparatus.....	4
Figure 1.2	Comparison of magnetic abrasive finishing (MAF) and magnetic fluid grinding (MFG).....	5
Figure 1.3	Typical magnetic fluid grinding apparatus.....	6
Figure 1.4	Design of permanent magnet float polishing apparatus.....	7
Figure 1.5	Schematic shows comparison between permanent magnet and electromagnet float polishing apparatus.....	8
Figure 2.1	Coats apparatus for polishing barrels [Coats, 1940].....	10
Figure 2.2	Schematic of typical magnetic fluid particle.....	12
Figure 2.3	Magnetic float polishing apparatus used by Umehara and Kato.....	13
Figure 2.4	Float forces for with and without a float, using permanent magnets.....	15
Figure 2.5	Relationship between removal rate and grinding load L	15
Figure 2.6	Relationship between the stock removal and the grinding time with and without a float.....	16
Figure 2.7	Relationship between removal rate and revolution speed.....	17
Figure 2.8	Relationship between removal rate and concentration.....	18
Figure 2.9	Relationship between removal rate and grain size.....	18
Figure 2.10	Relationship between sphericity and grinding time.....	19
Figure 3.1	Variation of buoyancy force with the height (Permanent magnets).....	23
Figure 4.1	Electromagnetic float polishing apparatus designed by Shinmura.....	26
Figure 4.2	Field conduction through electromagnetic float polishing apparatus.....	27
Figure 4.3	Comparison of an electromagnetic intensifier and permanent magnet apparatus.....	28

Figure 4.4	Field conduction for electromagnet and permanent magnet designs.....	28
Figure 4.5	Schematic of an electromagnetic polishing apparatus.....	30
Figure 4.6	Schematic of the electromagnetic power system.....	31
Figure 4.7a	Electromagnetic polishing apparatus and Bridgeport Machine tool.....	32
Figure 4.7b	Close up of the Electromagnetic polishing apparatus.....	32
Figure 4.8	Calibraton curve for electromagnetic float polishing.....	33
Figure 4.9	Float force for straight field electromagnetic float polishing apparatus.....	34
Figure 4.10	ANSYS electromagnetic model for straight field electromagnetic apparatus.....	35
Figure 4.11	B-H curver for mild steel in Tesla.....	36
Figure 4.12	B for straight field electromagnetic float polishing apparatus.....	38
Figure 4.13	H for straight field electromagnetic float polishing apparatus.....	39
Figure 4.14	B versus height for straight field electromagnetic apparatus.....	40
Figure 4.15	Variation of theoretical float force with height for straight field electromagnetic apparatus using ANSYS simulation.....	41
Figure 4.16	Ring pole electromagnetic float polishing apparatus.....	42
Figure 4.17	ANSYS model for ring pole apparatus.....	43
Figure 4.18	B plot for ring pole electromagnetic apparatus.....	44
Figure 4.19	H plot for ring pole electromagnetic apparatus.....	45
Figure 4.20	Geometric representation of the gap between ring pole and lower intensifier.....	46
Figure 4.21	Field strength for straight field and ring pole designs.....	47
Figure 4.22	Force versus height, h, for ring pole and straight field designs.....	48
Figure 4.23	Experimental and theoretical values for electromagnetic float polishing.....	50
Figure 5.1	Results of electromagnetic float polishing with convoluted intensifier...51	51
Figure 5.2	Magnetic field lines for a convoluted magnetic field intensifier.....	52
Figure 5.3	Upgraded magnetic field intensifier with water cooling system.....	53

Figure 6.1	Diameter and sphericity variation of Si ₃ N ₄ balls using an electromagnetic polishing test.....	56
Figure 6.2	The relationship between removal rate and revolution speed.....	57
Figure 6.3	Effect of abrasive type on material removal rate.....	58
Figure 6.4	The relationship between material removal and grain size.....	59
Figure 6.5	Variation of diameter and sphericity with time for electromagnetic float polishing.....	60
Figure 6.6	Initial sphericity of a silicon nitride ceramic ball.....	62
Figure 6.7	Final sphericity of a polished silicon nitride ball.....	63

CHAPTER 1

INTRODUCTION

1.1 Advantages of Advanced Ceramics

With increasing demand for efficient and technologically advanced systems, conventional engineering materials are pushed to new limits of operation. Steels, typically the workhorse of manufactured items, cannot function in developing technologies where high temperatures, high speed, high stiffness, and long reliable life are required. The trend towards advanced applications, such as turbochargers, jet engines, high speed spindles, gyros, X-ray, and chemical processing equipment requires new materials that can handle thermal, mechanical, and fatigue stresses that are encountered during operation of these systems.

Ceramic engineered components have the ability to perform in these areas. They are capable of high temperatures, high speeds, and corrosive environments that would damage other materials considered for installation. Table 1.1 shows a comparison of properties for silicon nitride bearing material and SUJ 2 bearing steel [Kurobe, 1992]. Silicon nitride, one of the leading engineering ceramics, is 60% less dense than M50 steel, has a Young's modulus of 45×10^6 psi compared to steel's 30×10^6 psi, and can operate at temperatures above 800 °C. Ceramic components typically require little lubrication, have up to 10 times longer life than steel components, and have lower heat generation during

Table 1.1 Comparison of properties between silicon nitride and SUJ 2 bearing steel

Properties	Silicon Nitride	Bearing Steel
Heat Resistivity °C	800	180
Density g/ml	3.2	7.8
Thermal Expansion 1/°C	3.2×10^{-6}	12.5×10^{-6}
Vickers Hardness kgf/mm ²	1700	800
Young's Modulus kgf/mm ²	3.2×10^4	2.1×10^4
Poisson's Ratio	0.26	0.20

operation than other bearing steels.

The advantages of ceramic components are evident and proven. However, the disadvantages of ceramics are of greatest concern to both manufacturers and the users. While having excellent hardness and wear properties, ceramics also have lower fracture toughness than steels. A silicon nitride ceramic component typically has a toughness of 6 MPa m^{1/2} for Si₃N₄ compared to 46 MPa m^{1/2} for steels. The fracture toughness drops drastically in a ceramic element containing small cracks or material flaws that increase internal stresses lowering material toughness. To reduce the chance of material failure, ceramic components must be free of flaws, contain high purity materials, and be highly polished to reduce cracks at the surface. The reduction of surface and subsurface cracks increases the experimental fracture toughness of ceramics allowing expanded capabilities and component reliability.

1.2 Conventional Production of Ceramic Components

Unfortunately, conventional production techniques for finishing ceramic balls require tumbling, rough lapping, and finish lapping, with high contact pressures, and hard abrasive grits that can scratch and damage the surface of the ceramic part. Hard abrasive grits can also cause deep, subsurface cracks that further reduce the ceramic's toughness. Conventional finishing techniques not only damage ceramic components, but also increase the cost of manufacturing ceramic parts.

Typical lapping processes require 1000s of ceramic balls polished simultaneously from a week to several weeks, raising the cost of ceramic parts. This finishing process can account for 50% of the total cost of the ceramic components limiting the potential of ceramics for new applications or for mass production. High cost and damage produced by conventional finishing techniques have spurred new technologies in high speed, low

damage finishing methods to accommodate the need for high precision, low cost ceramic elements.

1.3 New Finishing Techniques

Microcrack free regime grinding of brittle materials is a process with low contact forces, and lower surface damage than conventional lapping. However, this process requires a rigid, ultra-precision machine tool, using submicron superabrasive grinding wheels, to gently grind material from the surface of the ceramic parts, which are typically cylindrical. The main advantage of this process is the lower forces that reduce the surface and subsurface damage to the part. The disadvantages are the long process time, high capital expenditure for equipment, and production of singular components. Other methods of ceramic production are non-conventional in design, and represent recently available developments in polishing technology that incorporates existing equipment with high speed batch production of components.

Magnetic field assisted polishing is a method that originated in the U.S. during World War II for the purpose of polishing barrels [Coats, 1940]. The technology moved to the former U.S.S.R (Baron et al, 1975) and Bulgaria (Mekedonski et al, 1974) after the war where researchers developed the techniques into a wide range of applications. In the 1980's Japanese researchers followed this work and began developing techniques for finish polishing applications [Shinmura, 1985].

Magnetic field assisted polishing process utilizes a magnetic field and magnetic abrasive (magnetic material and abrasive) to remove material from the surface of a part. Figure 1.1 shows a typical magnetic abrasive finishing apparatus. The abrasive grits, through a magnetic media (solid or liquid), remove surface material with mechanical and/or chemical action due to the applied magnetic forces. In magnetic abrasive finishing (MAF) a

magnetic field conducted through the workpiece presses a “brush” of magnetic and abrasive particles against the workpiece.

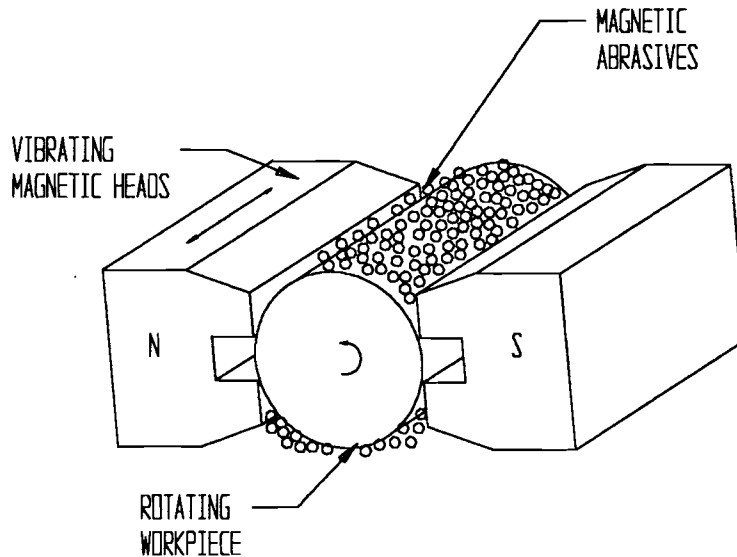


Figure 1.1 Schematic of the magnetic abrasive finishing apparatus

Material is removed as the workpiece is rotated inside the magnetic field and magnetic abrasive brush. The abrasive held stationary against the magnetic poles, scratch the surface of the workpiece removing the surface layer. The heads of the apparatus are reciprocated along the length of the workpiece to reduce the localization of abrasive grains on one area of the workpiece. The brush conforms to the shape of the workpiece allowing different sizes of cylinders to be polished without changing any of the equipment and the polishing pressure is maintained at a comparatively low value, typically around 5 psi. While magnetic abrasive finishing is excellent for rollers, a promising method for the production of spherical components, such as ball bearings or check valves, has been developed, known as “magnetic fluid grinding”, (MFG) or “magnetic float polishing” (MFP) [Tani, 1984].

Magnetic fluid grinding, or magnetic float polishing, is a magnetic field assisted polishing method that utilizes a fluid in the finishing process instead of magnetic abrasive

particles as in magnetic abrasive finishing. The concept behind the two methods is identical with magnetic particles generating the forces required to polish a moving workpiece. Figure 1.2 shows a conceptual comparison of magnetic abrasive finishing and MFG demonstrating the similarities and differences between the two methods. In magnetic abrasive finishing the abrasive grains are pressed against the workpiece as the magnetic particles exert force on the workpiece from the magnetic field. With MFG the magnetic fluid generates buoyant forces pressing the abrasive grains against the surface of the workpiece, causing the required material removal.

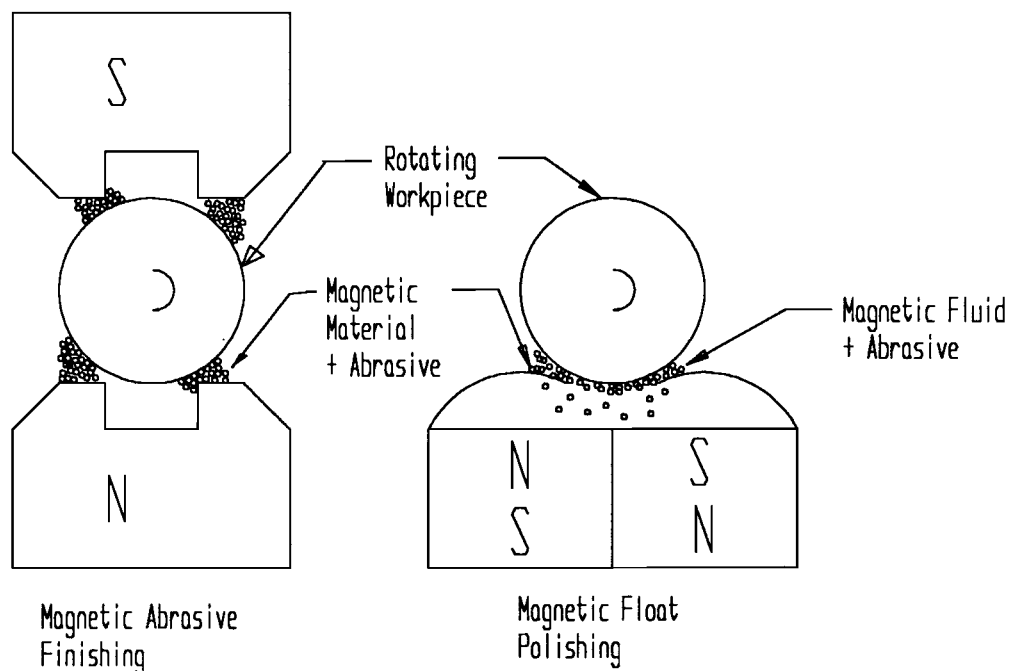


Figure 1.2 Comparison of magnetic abrasive finishing (MAF) and magnetic fluid grinding (MFG)

MFG promises to lower the cost of manufacturing ceramic bearing components through high speed, small batch production of quality finished ceramic parts. It typically polishes 10 to 20 balls, or roller bearings, simultaneously in under 6 hours and allows production of ceramic components of varying size without producing large quantities. This cost effective method has the potential to reduce the cost of the ceramic components while allowing greater flexibility during the production cycle.

A typical magnetic fluid grinding apparatus is composed of a magnetic fluid, abrasive particles, magnetic field, and a workpiece. The abrasive grains are suspended in the buoyancy of the magnetic fluid causing pressure by the abrasive against the workpiece. The workpiece is rotated through the magnetic fluid by either direct drive, or through the driving force of an external spindle. This type of apparatus is capable of polishing a wide variety of workpieces with complex geometries, including spherical balls. Typical magnetic fluid grinding equipment are represented below in Figure 1.3.

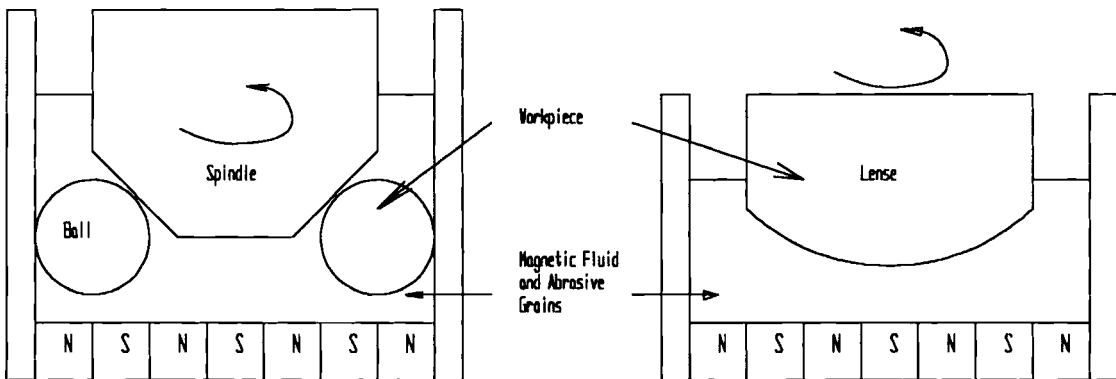


Figure 1.3 Typical magnetic fluid grinding apparatus

Magnetic fluid grinding has the advantage of operating on a wide range of shapes and sizes with little regard for the exact shape of the component. The system works equally well with spherical, concave, and convex surfaces such as balls, lenses, or mirrors that require smooth surfaces. However, the forces currently generated by the magnetic fluid limits the contact pressure that can be applied to the surface of the ball thus reducing damage to the surface of the ball during polishing.

1.4 Magnetic Float Polishing

Magnetic float polishing (MFP) is magnetic fluid grinding with the assistance of a float. A float plate, generally a light weight plastic, such as nylon, acrylic resin, or aluminum, stainless steel, or other non-magnetic material is placed inside the chamber below the workpieces. The balls to be polished are placed on the periphery of the chamber and a drive spindle is placed above the balls. The chamber is filled with a magnetic fluid that generates buoyancy forces inside the polishing chamber due to the externally imposed magnetic field.

A magnetic fluid is a colloiddally dispersed magnetic solid, typically magnetite, that is maintained inside a carrier fluid, hydrocarbon or water, that generates a pressure gradient due to an imposed magnetic field. The magnetic fluid is characterized by a field strength, or magnetization, which depends on the concentration of the magnetite particles inside the carrier fluid. A typical magnetic fluid magnetization is 600 gauss.

Free abrasive is added to the magnetic fluid, typically 1-5 ml of abrasive, and the drive spindle is operated causing the balls to rotate through the magnetic fluid and abrasive causing material removal. Figure 1.4 shows a diagram of a typical MFP process. The advantage of MFP is the low polishing force, which prevents scratching, and high speeds which can lower manufacturing time considerably.

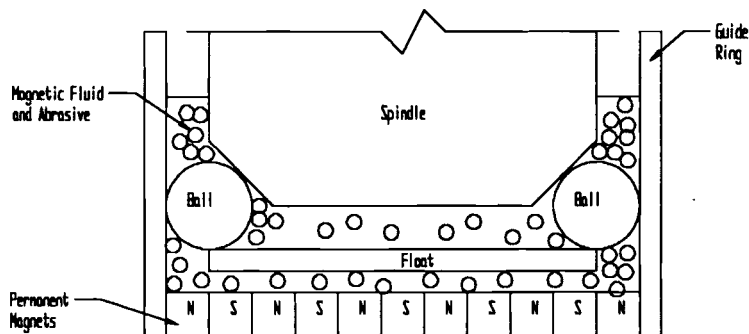


Figure 1.4 Design of permanent magnet float polishing apparatus

MFP relies on magnetic fluid and a magnetic field to generate the buoyant forces inside the polishing chamber. While magnetic fluids can be varied in conventional MFP, the magnetic field is typically generated from a set of permanent magnets positioned under the polishing chamber which generates a static magnetic field inside the polishing chamber. One way to alter the characteristics of MFP is to alter the shape and strength of the magnetic field that generates the buoyancy forces inside the polishing chamber.

Electromagnetic float polishing is an effort to alter the generation of magnetic fields used in MFP, and to change the buoyancy forces inside the polishing chamber. Figure 1.5 shows a comparison of permanent magnet and electromagnet equipment for the polishing of ceramic ball bearings.

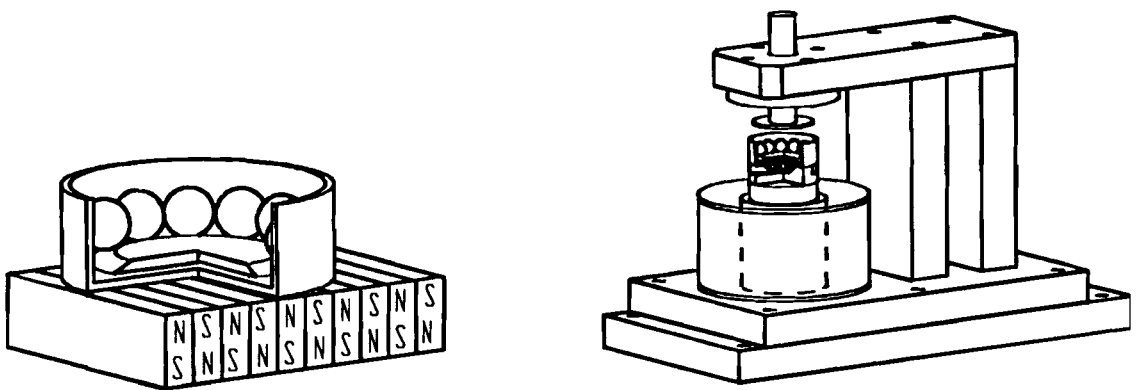


Figure 1.5 Schematic shows comparison between permanent magnet and electromagnet float polishing apparatus.

While the permanent magnet apparatus has a specific geometry of magnets, the electromagnet machine has a magnetic field intensifier that can alter the shape of the magnetic field. The magnetic coil can alter the strength of the magnetic field while pol-

ishing allowing the apparatus to be used from roughing to the final polishing operation without changing the equipment, or stopping the polishing process. The difference between the two methods makes it possible for an electromagnet apparatus to offer capabilities in magnetic fluid grinding that have not been previously explored.

CHAPTER 2

LITERATURE REVIEW

2.1 Origin of Magnetic Field Assisted Polishing

One of the earliest accounts of magnetic field assisted finishing is by Coats (1940). He produced a machine to polish barrel shells by placing a magnet near the outside of a barrel and putting magnetic abrasive grits inside while the barrel is rotated. This apparatus was the precursor for developments in internal polishing and for the technology that arose in East European research facilities chiefly from the former U.S.S.R. and Bulgaria after World War II. The apparatus constructed by Coats is shown in Figure 2.1.

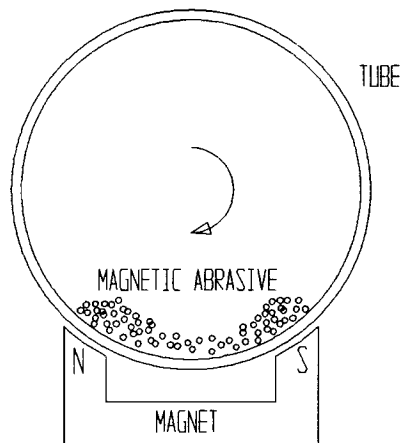


Figure 2.1 Coats apparatus for polishing barrels [Coats, 1940]

This technology was used in the former U.S.S.R. by Baron (1975) and his associates along with a Bulgarian researcher, Mekedonski (1974). Japanese researchers Takazawa, Shinmura, and Hatano (1983, 1985) later utilized concepts developed by Baron and Mekedonski to develop methods for polishing steel rollers. Shinmura (1989a) and Baron (1986) also polished the inside of non-ferromagnetic tubes using higher speeds than Coats, developing methods to polish internal ceramic surfaces efficiently.

Shinmura also used magnetic field assisted finishing to produce smooth finish (R_{max} of

0.2 μm) on external surfaces with the use of magnetic abrasive and strong magnetic fields. He has shown methods to polish ferromagnetic cylinders [Shinmura, 1985a], and finishing plane surfaces [Shinmura, 1985d] in addition to the work done on internal surfaces. Other researchers expanded the use of magnetic field assisted finishing to flat and curved surfaces that could not be rotated allowing enhanced versatility for the polishing process [Shikhirev et al., 1980].

The similarity between all of these individual pieces of equipment is the use of a mixture of magnetic particles and dry abrasive to polish the workpiece. The magnetic particles are typically large domain iron with the abrasive either loosely mixed or sintered to the magnetic particle.

Shinmura (1987) studied the effect of polishing with white alumina oxide (WA) and iron particles, altering the method of combining the iron and abrasive grains, i.e. sintering and reaction bonding. Shinmura also found improvement in polishing efficiency with the addition of a fluid, yielding 30 times improvement in stock removal [Shinmura, 1986]. One variable that Shinmura did not vary was the use of nanometer size magnetic particles in a liquid suspension. This combination allows higher mobility of abrasive particles and becomes magnetic fluid grinding. However, the magnetic fluid needs to be recovered as it is rather expensive.

2.2 Magnetic Fluid Grinding

One of the first uses of magnetic fluid as a polishing media was reported by Tani at the University of Tokyo, Japan (1984). Tani used a magnetic fluid made of colloidal dispersed subdomain particles of a ferrimagnetic material, typically magnetite Fe_3O_4 to polish acrylic resin. The magnetic fluid and the concepts of buoyancy used by Tani in this paper was originally developed by Rosensweig (1966b) and later patented

[Rosensweig, 1970]. Figure 2.2 shows a schematic of typical magnetic fluid particles. The particles in the magnetic fluid are maintained colloidally due to Brownian (thermal) motion with the assistance of a surfactant to prevent the separate magnetic particles from agglomerating under van der Waal's forces. The combination of a suitable surfactant to the surface of the magnetite and a suitable carrier fluid allows a stable magnetic fluid utilized in Tani's experiments.

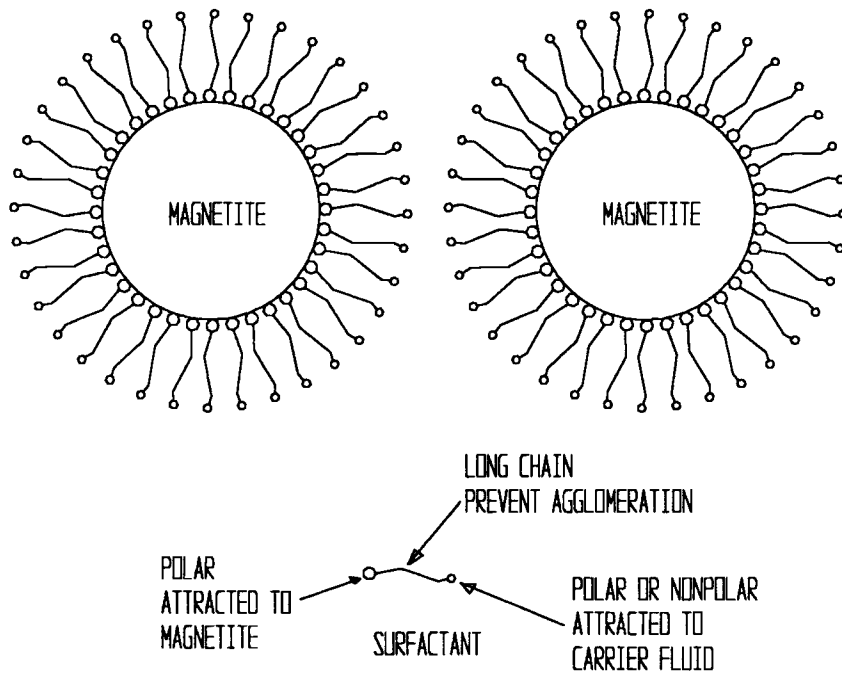


Figure 2.2 Schematic of typical magnetic fluid particle

Magnetic fluid, with 2-10 nm magnetic particles, is drawn to the magnetic field gradients causing nonmagnetic items inside the magnetic fluid to be buoyantly levitated [Rosensweig, 1966a]. As the nonmagnetic particles are forced upward they are pushed against the workpiece causing material removal. Tani found, through his experiments, that acrylic resin could be polished removing 2 $\mu\text{m}/\text{min}$ with a silicon carbide abrasive. Magnetic fluid grinding is similar in concept to the idea developed by Baron and later Shinmura in as much as the work concerns using dry magnetic abrasive.

While Tani's experiments show promise for the finishing of non-traditional materials,

his development had poor form control. To improve the capabilities and shape control of Tani's original design, Umehara and Kato (1990) developed a system of magnetic fluid grinding with the assistance of a buoyant float. The added float in magnetic float polishing increases the forces imposed on the workpiece and improves the sphericity of ball components.

2.3 Magnetic Float Polishing

Umehara and Kato polished cold isostatically pressed silicon nitride ball blanks of about 9 mm diameter with silicon carbide abrasive grains. A diagram of their polishing apparatus is shown in Figure 2.3. The polishing apparatus consisted of a high speed spindle (capable of 20,000 rpm), a magnetic fluid with 400 Gauss magnetization, and an acrylic resin float. The magnetic field required to generate the buoyant force during polishing was produced by a set of permanent magnets of 4 mm square, assembled with alternating polarities. This configuration give a magnetic field strength of 9.2×10^5 A/m and a field gradient of 1.4×10^7 A/m².

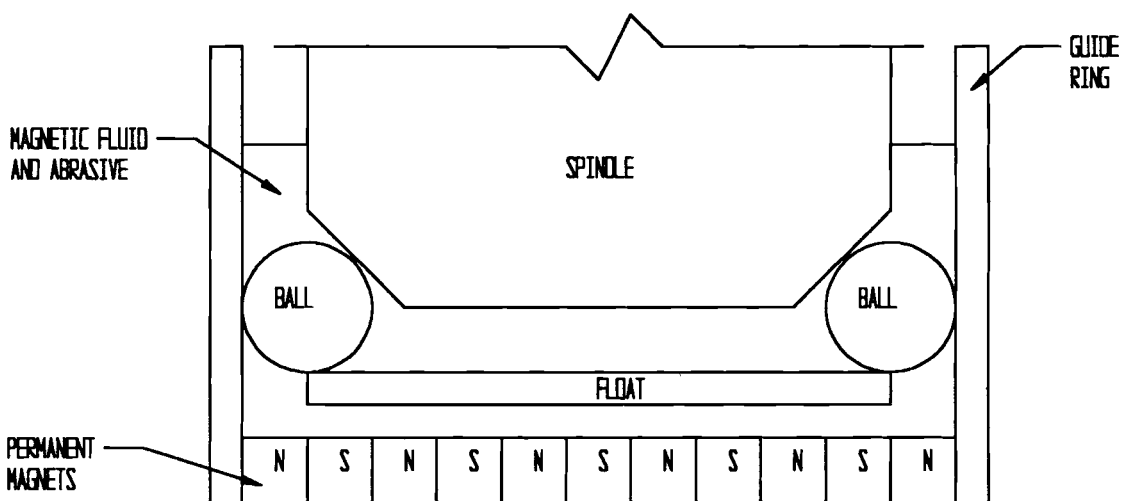


Figure 2.3 Schematic of magnetic float polishing apparatus used by Umehara and Kato (1990)

During these experiments it was shown that, with the addition of a float, the float grinding load could be increased from 2 N without a float to over 6 N with the float. Since the removal rate is proportional to grinding load, the float improves the material removal capabilities of the apparatus. A comparison between the use of a float and without a float shows the advantages gained with this innovation. Table 2.1 shows differences in magnetic float polishing when polishing cold isostatically pressed silicon nitride. The float results were obtained with an acrylic resin float. The magnetic fluid is a water based fluid with 400 G magnetization.

Table 2.1 Comparison between MFP with and without the addition of a float.

	With Float	Without Float
Maximum Grinding Load, N	5.7	1.7
Removal Rate at 0.7 N, $\mu\text{m}/\text{min}$	3.6	1.6
Maximum Removal Rate, $\mu\text{m}/\text{min}$	12.4	2.2

2.4 Variables in Magnetic Float Polishing

Umehara and Kato [1990] conducted research on the effect of individual polishing variables on the stock removal rate, final surface finish, and sphericity. This research is the basis for understanding new possibilities in magnetic float polishing. Umehara and Kato have recognized the influence of the following variables in magnetic float polishing.

- * Total grinding load 7 N
- * Rotational Speed 1000 - 20000 rpm
- * Concentration of Abrasive Grains 10 % - 40 % by volume
- * Abrasive Grain Size up to 200 μm

The variation of buoyant force with the distance above the bottom of the polishing

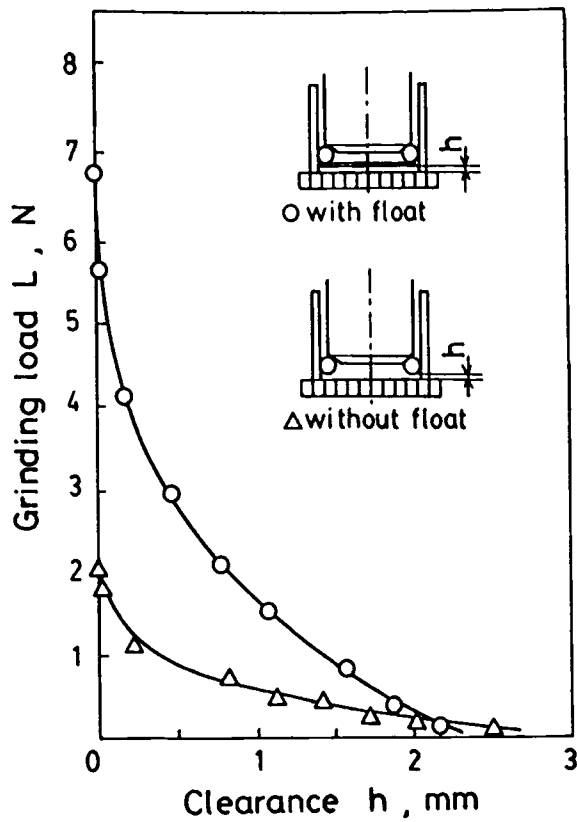


Figure 2.4 Float forces with and without a float, using permanent magnets [Umehara and Kato, 1990].

The benefit of the float is the increased grinding load or float force. The higher float forces cause increased material removal as shown in Figure 2.5.

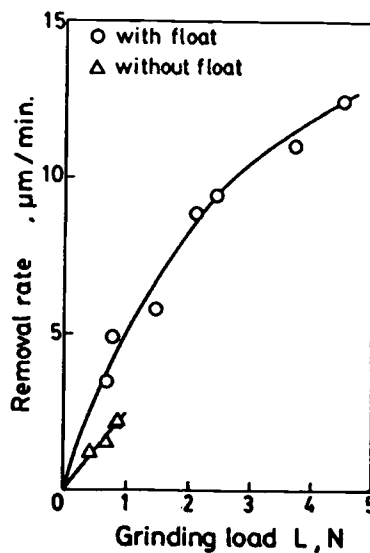


Figure 2.5 Relationship between removal rate and grinding load L [Umehara and Kato, 1990].

The addition of the float in magnetic fluid grinding increases the maximum removal rate of Tani's experiments of 2 $\mu\text{m}/\text{min}$ to 12 $\mu\text{m}/\text{min}$, allowing faster production times and increased finishing efficiency. Then, the addition of the float greatly improves the overall stock removal process over time as shown in Figure 2.6.

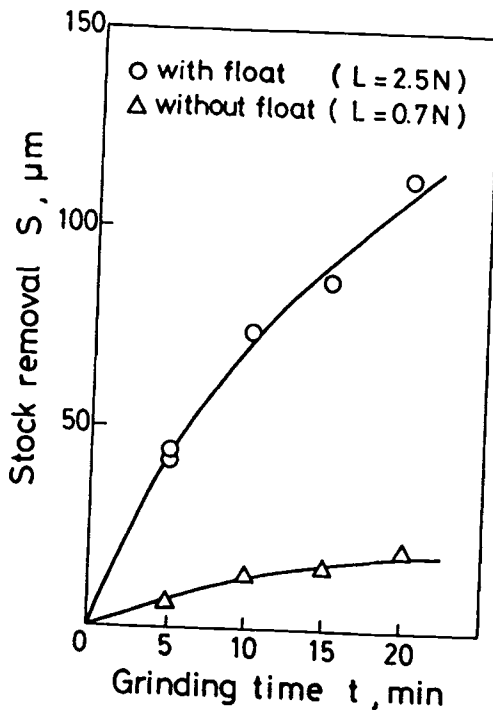


Figure 2.6 Relationship between the stock removal and the grinding time with and without a float [Umehara and Kato, 1990].

The removal rate in Umehara's experiments were also found to be a function of the rotational speed of the drive spindle. Figure 2.7 shows the variation of speed for different loading situations. The removal rate appears to increase exponentially with rotational speed to a critical speed of approximately 9000 rpm in Umehara's experiments.

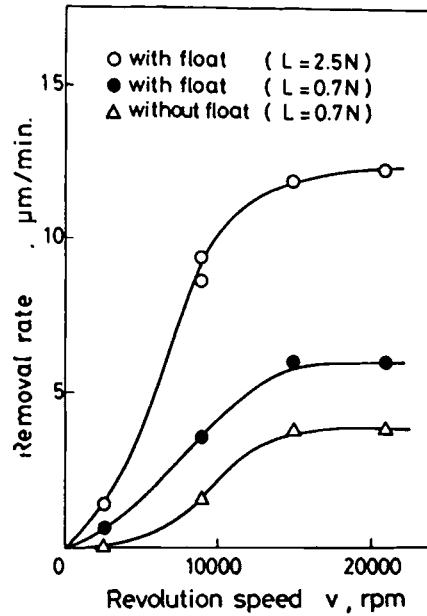


Figure 2.7 Relationship between removal rate and revolution speed [Umehara and Kato, 1990].

Figure 2.8 shows the variation of removal rate with concentration of abrasive in the magnetic fluid. It shows a rapid increase in removal rate up to a concentration of 10% followed by saturation. It is apparent that a concentration of about 10 volume percent is optimum.

Figure 2.9 shows the variation of removal rate with grain size of the abrasive. It shows an increase in removal rate to a maximum near 10 $\mu\text{m}/\text{min}$. The removal rate is found to be constant with abrasive grains in the range of 200 μm .

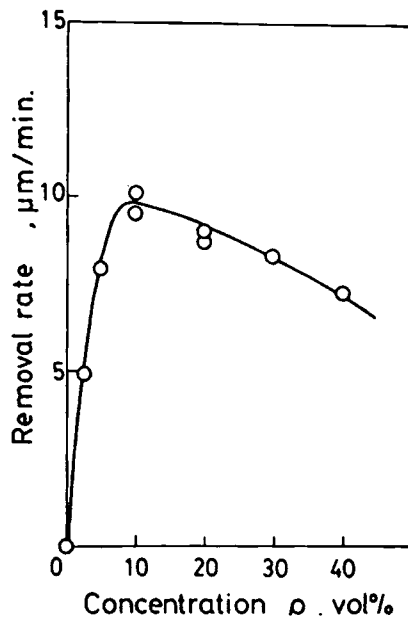


Figure 2.8 Relationship between removal rate and concentration [Umehara and Kato, 1990].

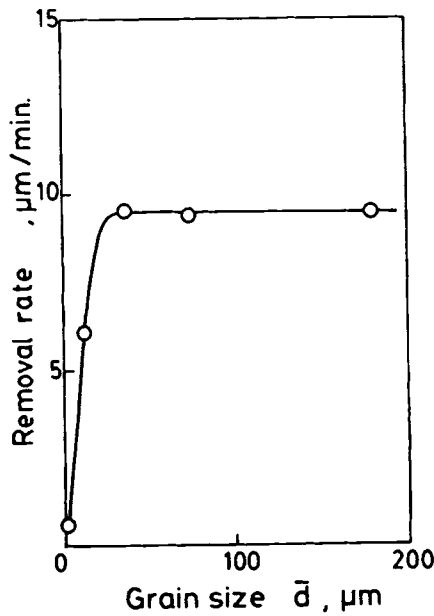


Figure 2.9 Relationship between removal rate and grain size [Umehara and Kato, 1990].

Another improvement with the float is control of sphericity. Umehara and Kato report an increase in sphericity, or increasing form error, without a float. However, with the addition of a float to the polishing process, the sphericity of the ceramic ball dropped

from 500 μm to a minimum of 0.14 μm allowing magnetic float polishing to produce quality formed parts [Umehara and Kato, 1990]. Figure 2.10 shows the relationship between sphericity and grinding time t , for Umehara's experiments. These experiments also report excellent surface finish.

The original surface roughness of the ceramic blank was 10 μm R_{max} (i.e. measured from highest point to lowest valley), this roughness was lowered to 0.1 μm R_{max} after 180 min of polishing time. It was found that the removal rate for this polishing process increased with rotational speed achieving a maximum at 9000 rpm. Above this speed, the removal rate is constant.

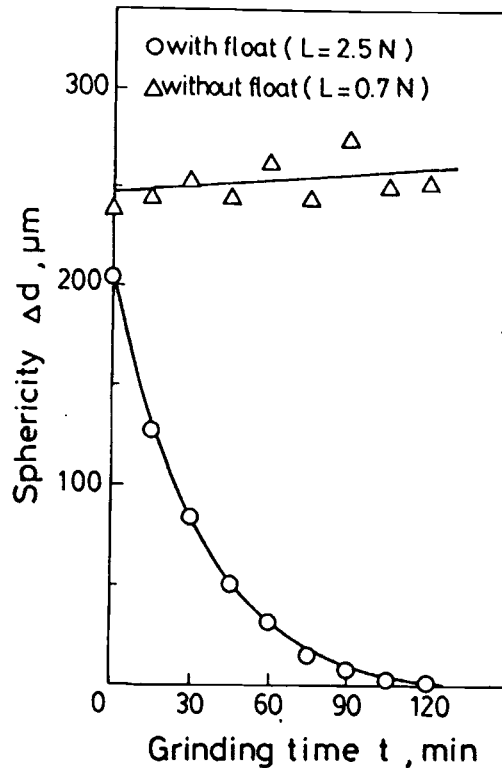


Figure 2.10 Relationship between sphericity and grinding time [Umehara and Kato, 1990].

2.5 Theoretical Considerations

Further theoretical studies of magnetic float polishing was undertaken by Childs et al (1994). They developed theoretically the volume removal rate for sliding contact during float polishing. This calculation is based on experiments that fit the abrasive wear law (Archard's wear law).

$$V = \frac{K W v}{H}$$

K - Wear Constant
W - Polishing Load

v - Sliding Velocity
H - Hardness of Workpiece
V - Volume Removal Rate

Childs et al (1994) utilized this equation, with assumptions about the ball motion under conditions of rolling and sliding to generate a wear equation with variables pertinent to magnetic float polishing.

$$\text{Volume Removed} = 0.54 \frac{K}{H} (\omega b \sin \beta + \Omega f) W_m^{4/3} \left(\frac{rb}{E}\right)^{1/3}$$

K -wear coefficient
H -workpiece hardness
 ωb -ball spin angular velocity
 β -angle of ball spin axis

W_m -contact load
rb -ball radius
E -Young's modulus
 Ωf -float angular velocity

Experiments performed showed that the sliding speed between the ball and the top plate generates the predominate amount of material removal. Therefore, large sliding velocities are favored for increased efficiency. The rotational speed at which sliding begins to occur was found to depend on the contact between the top plate and the ball and the viscosity of the magnetic fluid. The highest sliding speed obtained, 7 m/s, yielded a removal rate of 7 $\mu\text{m}/\text{min}$. A wear coefficient of 0.070 ± 0.02 was estimated for this

experiment. This wear coefficient is indicative of 2-body abrasion caused by abrasive grits embedded in the drive shaft of the polishing apparatus which is expected with hard abrasive grits sliding between the workpiece and the drive plate (typically made of soft materials).

While the work of Umehara and Kato (1990) and Childs et al (1994) show the advantages of magnetic float polishing, areas of magnetic float polishing have yet to be explored. Shinmura (1989 b) has shown that an electromagnetic polishing apparatus is feasible if a strong magnetic field can be generated in the polishing area. This concept of using an electromagnetic field to float polish is a natural step in the development of a system for efficient polishing of ceramic ball components.

CHAPTER 3

PROBLEM STATEMENT

3.1 Advantages of Magnetic Float Polishing

Magnetic float polishing is a process that has the potential for lowering the cost of manufacturing ceramic elements significantly. The technology accommodates variation in ball sizes which are polished to the same size, in small batch sizes, and can be altered to operate on a production scale with minor modifications. The low cost of silicon carbide and inexpensive construction materials also lower the capital cost of magnetic float polishing.

The magnetic fluid is currently the most expensive part of the magnetic float polishing but the price probably can come down significantly with increase in volume use.

Unfortunately, at this time, the markup for research and development cause the fluid to be sold for over \$500/liter. This is partly because test fluids are used in small quantities for application, such as speakers, seals, and bearings. For polishing application where a significant amount of magnetic fluid is needed, MFP will be economically viable only when magnetic fluid is available at nominal cost.

It should be noted that magnetic float polishing does not require any complex equipment. The single greatest investment is a precision high-speed spindle capable of operating in the speed ranges required. Other equipment is easily fabricated in a standard metal working shop.

The earlier experiments on magnetic float polishing were performed using a set of permanent magnets arranged with alternating N and S poles to yield high field strength and high field gradients. While this method works well for polishing, the possibility of

improving the magnetic float polishing system has led to interest in generating stronger magnetic fields.

A typical permanent magnet apparatus can generate buoyancy forces near 7 N and stiffness values close to 4 N/mm. The force vs position curve for a typical permanent magnet float polishing apparatus is determined by the geometry and strength of the permanent magnets and can not be altered. This limitation is evident when attempting to achieve higher forces with lower stiffness, which could allow excellent finish polishing of equipment previously polished for form.

Figure 3.1 shows the limitation of a permanent magnet apparatus in the buoyancy plot of a typical permanent magnet apparatus. A force plot, which shows the sum of contact loads on all the balls in the polishing chamber when the balls are located at a particular height from the bottom yields the sum of contact forces on the workpieces.

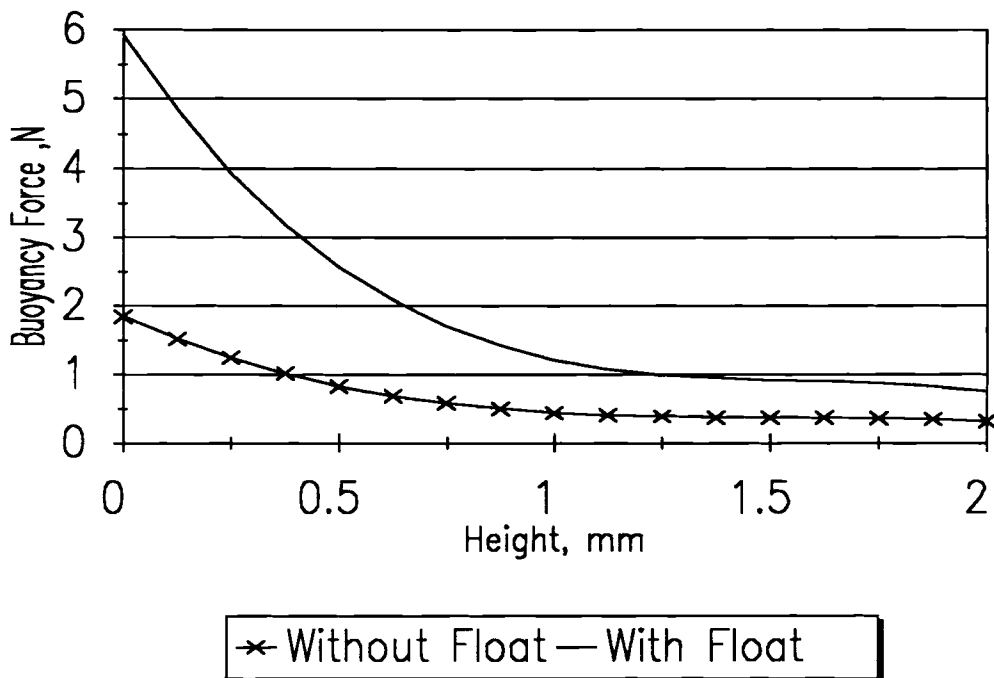


Figure 3.1 Variation of buoyancy force with the height (Permanent magnets)

3.2 Electromagnetic Float Polishing

An electromagnetic apparatus is very similar in principal to a permanent magnet system. The magnetic field is generated by passing current through a copper coil placed around a low carbon steel core. The coil, when energized with high current provides a magnetic field to the inside of the polishing chamber instead of permanent magnets, where magnetic fluid buoyancy acts on the abrasive grains, the float, and the workpiece. The major difference between the two designs is the shape of the magnetic field inside the chamber.

An electromagnetic apparatus can produce a stronger magnetic field than current permanent magnet technology (0.6 Tesla for permanent magnets and 1.8 T for an electromagnetic apparatus). However, the electromagnet required to generate these stronger fields is quite large compared to the small permanent magnets used in typical polishing equipment. For this reason, the electromagnet apparatus is physically larger than the permanent magnet equipment.

The theoretical advantage of an electromagnetic float polishing apparatus is the possibility of high field strengths and large field gradients, which can produce higher removal rates than with permanent magnets. The higher field gradients could also improve the form error associated with the production of ceramic balls for bearing applications. With the possibility of improving magnetic float polishing technology, electromagnetic equipment is a logical step in the continuation of previous polishing experiments.

CHAPTER 4
ANALYSIS AND INITIAL EVALUATION
OF MAGNETIC FLOAT POLISHING

4.1 Initial Design

Electromagnetic float polishing is a new field of fluid assisted polishing as originally proposed by Tani (1984). While Tani's experiments, and those that followed, show promise for improving the capabilities of polishing ceramic workpieces, all of these methods have utilized permanent magnets to generate the magnetic fields that cause buoyant forces. Electromagnets show promise because of the added flexibility that can be incorporated into the design of the polishing apparatus. The electromagnet machine is not limited to the restraints of permanent magnets such as geometry or strength, and can be incorporated into new shapes and capabilities.

One design for an electromagnetic polishing apparatus was developed by Dr. Shinmura of Japan [Shinmura, 1992]. Shinmura expanded on a permanent magnetic design by incorporating similarities between the permanent and electromagnetic designs. The permanent magnet apparatus has a specified magnetic field strength, typically 0.6 T. This same magnetic field strength was used to calculate the minimum current and wire turns used in the electromagnetic coil during the design of the electromagnetic apparatus. The electromagnetic machine was then designed around the maximum magnetic flux through all of the steel components to minimize the magnetic field losses during operation.

Figure 4.1 is a schematic of the electromagnetic float polishing apparatus, incorporating an electromagnetic coil, low carbon steel core for the conduction of the magnetic field, steel intensifiers to position the magnetic field, and an area designed to place a polishing

chamber. These separate components work together to generate the required field strength, and gradient, and to generate the buoyancy forces required for efficiently polished ceramic component.

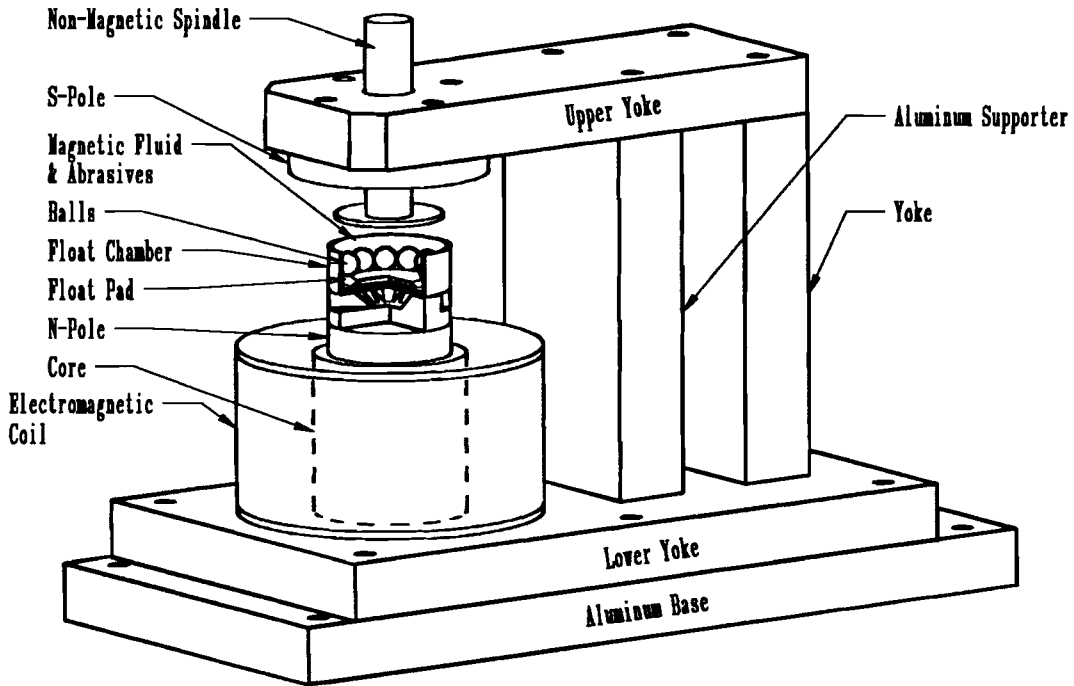


Figure 4.1 Electromagnetic float polishing apparatus designed by Shinmura

The expected field conduction through this apparatus can be seen in Figure 4.2. It shows the magnetic field generation in the copper coil of the electromagnetic machine, and the field conduction through the steel magnetic field conduction plates, and finally through the polishing chamber.

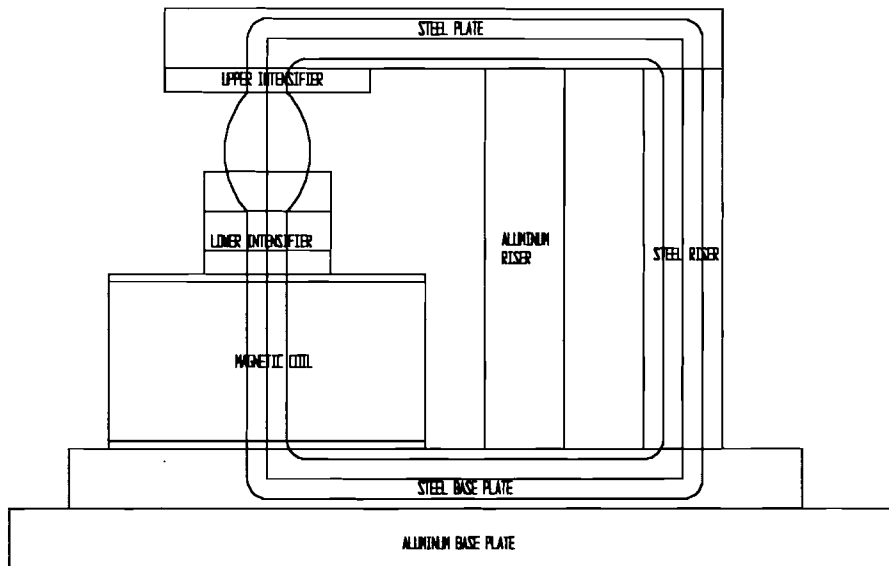


Figure 4.2 Field conduction through electromagnetic float polishing apparatus

The magnetic field is conducted through the magnetic coil, the steel base plate, up through the steel riser, across the steel top plate, and through the upper intensifier. The lower intensifier, just above the magnetic coil, is responsible for the shape, and gradients of the magnetic field dispersed through the polishing chamber and greatly influences the polishing characteristics of the equipment.

Figure 4.3 is a comparison of a convoluted electromagnetic field intensifier, and a permanent magnet apparatus with alternating fields. While the gap between the two intensifiers determines the field strength, the upper and lower field intensifiers determine the field gradient. Therefore, the shape of the lower field intensifier directly under the polishing chamber determines the field gradients and the strength of the buoyant forces inside the polishing chamber. The initial design of the lower field intensifier resembles somewhat the design of a permanent magnet apparatus with alternating north and south magnetic poles.

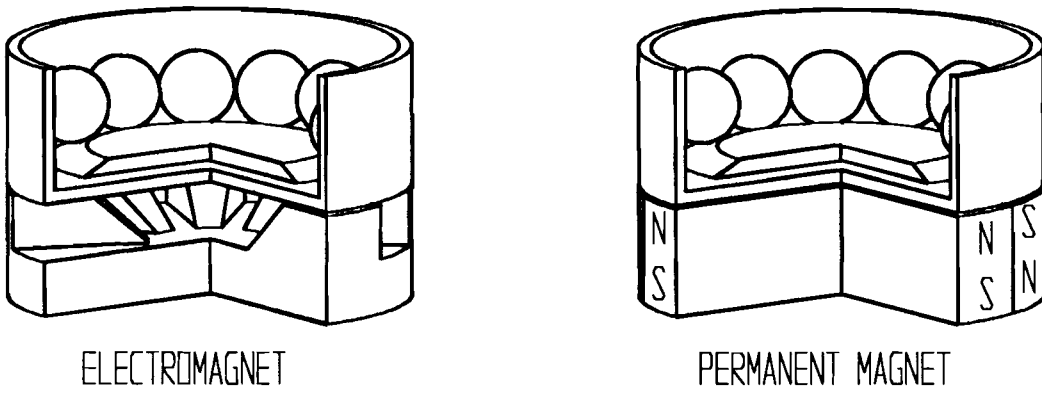


Figure 4.3 Comparison of an electromagnetic intensifier and permanent magnet apparatus

The similarity shows the intent of the designer in attempting to reflect the field gradients of the permanent magnet equipment into an electromagnetic apparatus. The cut out sections of the electromagnetic intensifier simulate the change in magnetic field direction inherent in the permanent magnet machine.

Figure 4.4 shows the magnetic field lines from these two configurations. The electromagnetic intensifier on the left is from the electromagnetic apparatus and generates strong and weak magnetic fields orientated in the same direction. However, the permanent magnet apparatus on the right generates alternating magnetic fields that are restrained to the surface of the magnets, generating extremely high magnetic field gradients.

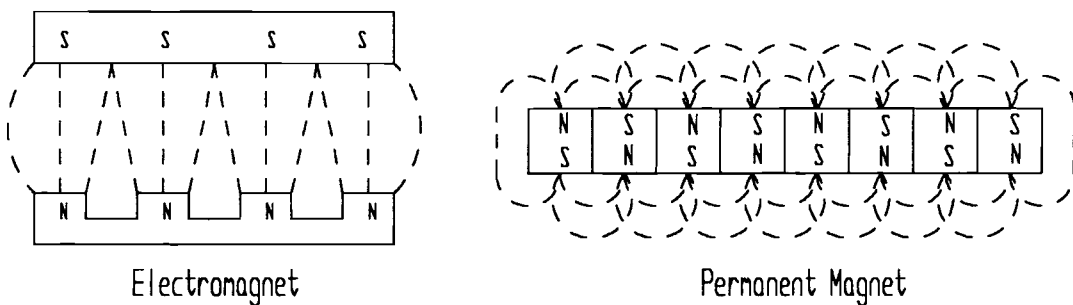


Figure 4.4 Field conduction for electromagnet and permanent magnet designs

It can also be seen from the figure that in electromagnetic design the field conducts straight through the polishing chamber, which rests on the north poles, and in a perma-

ment magnet system the magnetic field is reversed within the lower portion of the float polishing chamber. The difference between these two designs yields the possibility of new polishing capabilities due to the

4.2 Construction of Electromagnetic Polishing Apparatus

The electromagnetic polishing apparatus was constructed for this investigation from designs developed by Shinmura of Japan. The drawings were originally hand drawn by Shinmura and later transferred to CADKEY for permanent storage. The drawings, as developed in CADKEY, are given in Appendix A.

Figure 4.5 shows a schematic of the electromagnetic polishing machine. The apparatus is divided into nine parts. First is an aluminum (6061-T6) base plate. The purpose of the aluminum base plate is to separate the steel base plate containing the magnetic field from the machine base. Since the spindle has a steel table (the Bridgeport machine tool, in this case) the steel base plate of the electromagnetic machine must not contact the steel machine tool table. If the steel base and steel table were allowed to touch, magnetic field leakage would reduce the effectiveness of the polishing apparatus.

The steel base plate serves as the magnetic linkage between the magnetic core and the steel riser. The magnetic field is conducted through the base plate up through the steel riser (which is located at the rear, away from the coil) of the machine. The steel riser is placed in this location to minimize leakage between the lower intensifier (which rests on the coil) to the riser. If the riser is too close to the lower intensifier the magnetic field would conduct to the riser causing asymmetric field propagation through the polishing chamber.

The aluminum riser, which is identical in geometry to the steel riser, is only used to reduce the cantilever effect of the steel top plate. The steel top plate conducts the field from the steel riser to the upper intensifier which directs the magnetic field to pass through the polishing chamber.

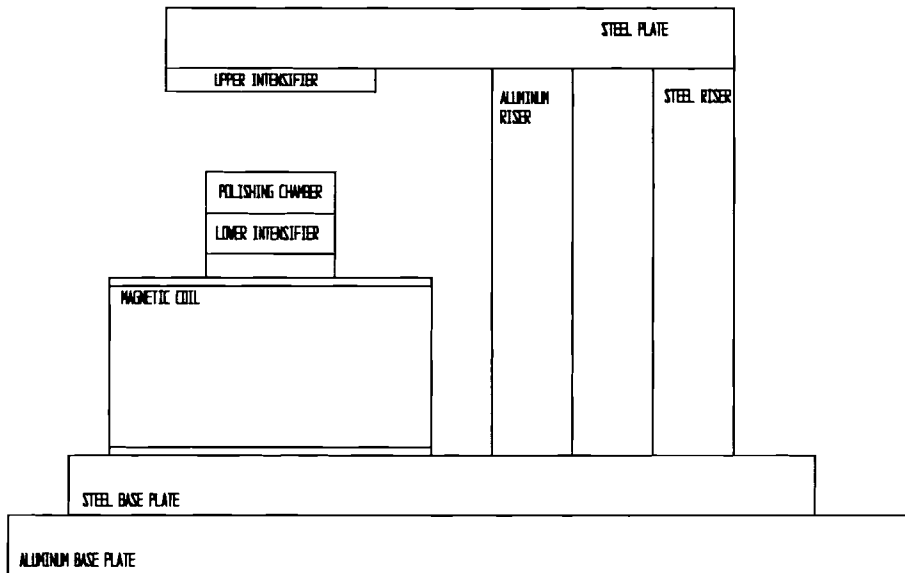


Figure 4.5 Schematic of an electromagnetic polishing apparatus.

The magnetic coil generates the magnetic field for the polishing of the ceramic ball elements. The magnetic coil in this apparatus is constructed of three separate magnetic coils. Each coil has 1800 turns of 10 AWG insulated copper wire. The three coils combined have 5400 turns total, with each of the three coils having 3 Ω of resistance.

Figure 4.6 shows a schematic of the electromagnetic power system used. The magnetic coils are energized with three separate power supplies. Each power supply produces 24 V and up to 6 A continuous current. The power to the magnetic coils is controlled with three separate Apex PA12 op-amp circuits that regulate the voltage to the magnetic coils. The power from the op-amps are passed through three full-wave bridge rectifiers to maintain proper polarity and to protect the op-amps from voltage backlash that is generated when the power is quickly removed from the inductive magnetic coils.

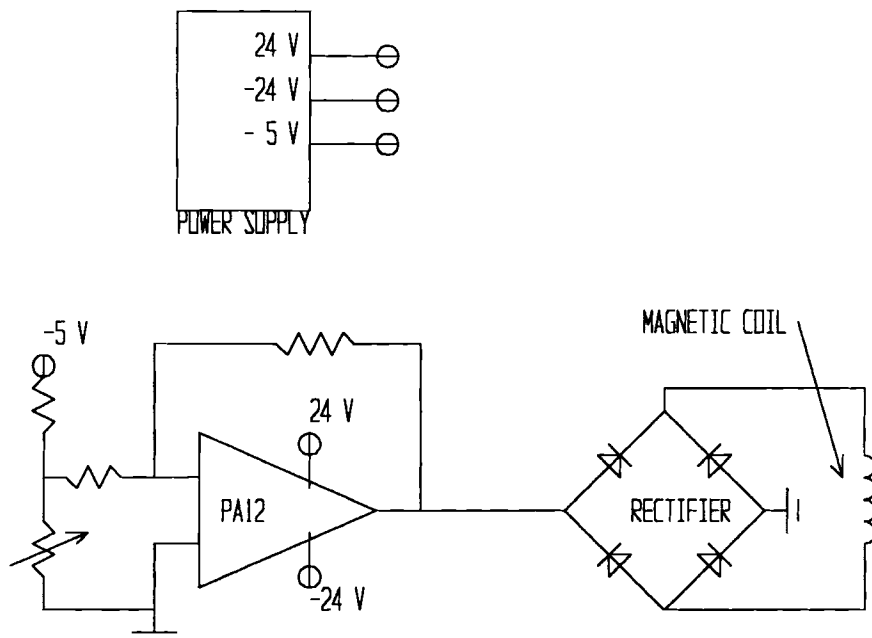


Figure 4.6 Schematic of the electromagnetic power system.

The power output from the op-amps is controlled with a potentiometer that regulates the voltage inputs into the op-amp circuit. For monitoring purposes, three current meters are used to determine the actual current flow through each of the three separate magnetic coils. The total magnetic field generation is then determined with a teslameter at the upper surface of the magnetic core. Photographs of the electromagnetic float polishing apparatus on a Bridgeport machine tool shows, in Figure 4.7 (a) and (b), showing various elements in this apparatus.

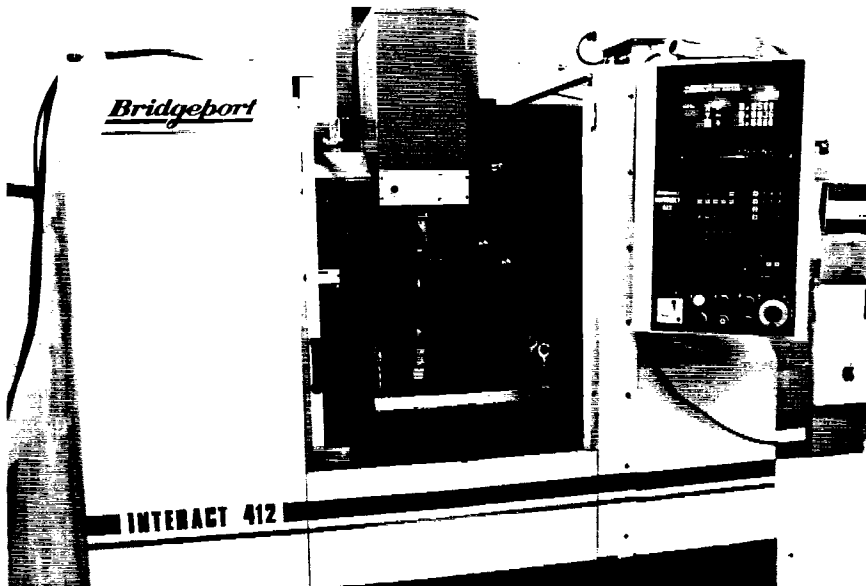


Figure 4.7a Electromagnetic polishing apparatus on a Bridgeport Machine tool

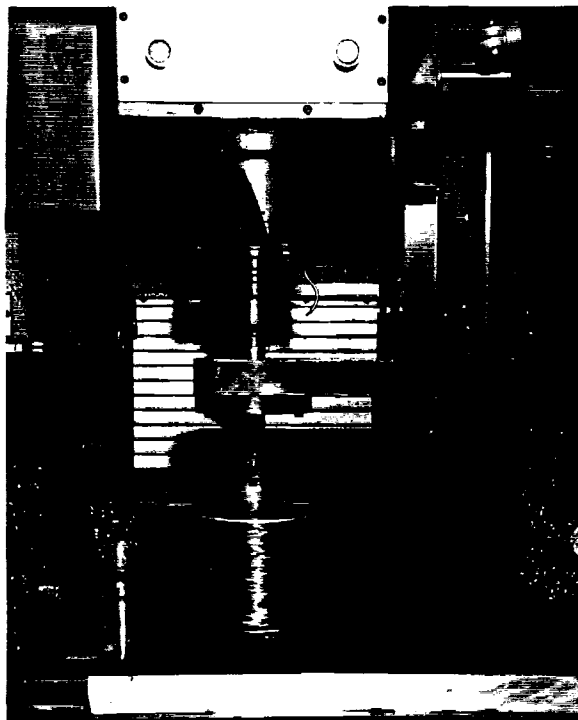


Figure 4.7b Close up of the Electromagnetic polishing apparatus

4.3 Initial Evaluation

The electromagnetic float polishing apparatus was constructed and tested to determine the float force inside the polishing chamber. For testing the apparatus was placed on a 3-axis Kistler piezoelectric dynamometer. The dynamometer was connected to a Kistler charge amplifier and voltmeter so that force measurements could be determined. A calibration curve was generated using 0.50 lb and 1.13 lb weights. A calibration curve of voltage versus force is shown in Figure 4.8.

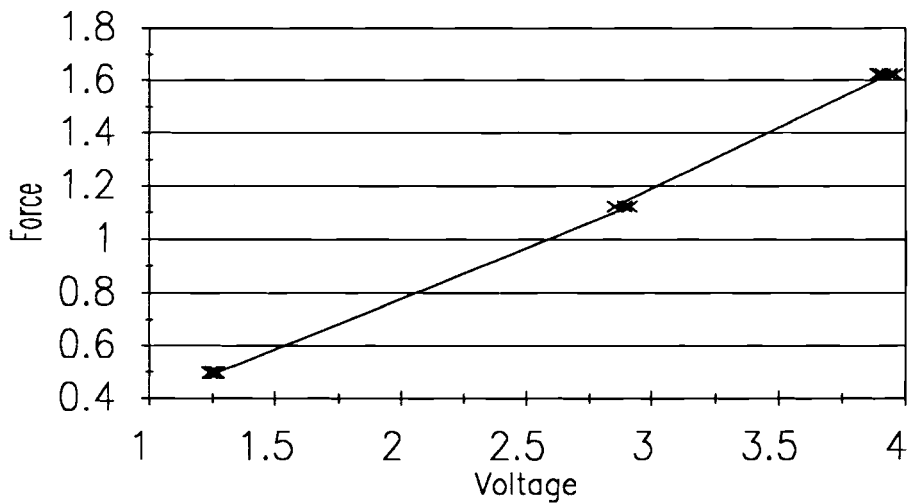


Figure 4.8 Calibration curve for the dynamometer in electromagnetic float polishing apparatus

This calibration curve was generated by placing weights on the apparatus while monitoring the voltage output of the charge amplifiers. The magnetic coil during calibration was not charged, but, it was found that when the magnetic coil is charged, subtle corrections, around 10 %, must be made to account for the magnetic coil's tendency to decrease in weight as the spindle is lowered toward the magnetic coil. The force plots will actually decrease as the magnetic leakage conducts from the magnetic coil to the steel spindle of the Bridgeport.

Once the calibration curve was generated the buoyant forces of the polishing apparatus could be determined. Figure 4.9 shows the variation of buoyant force for a 12.5 mm thick nylon float, nylon balls approximately 12.5 mm in diameter (about the size of a Si₃N₄ balls), and a thin top plate to apply forces.

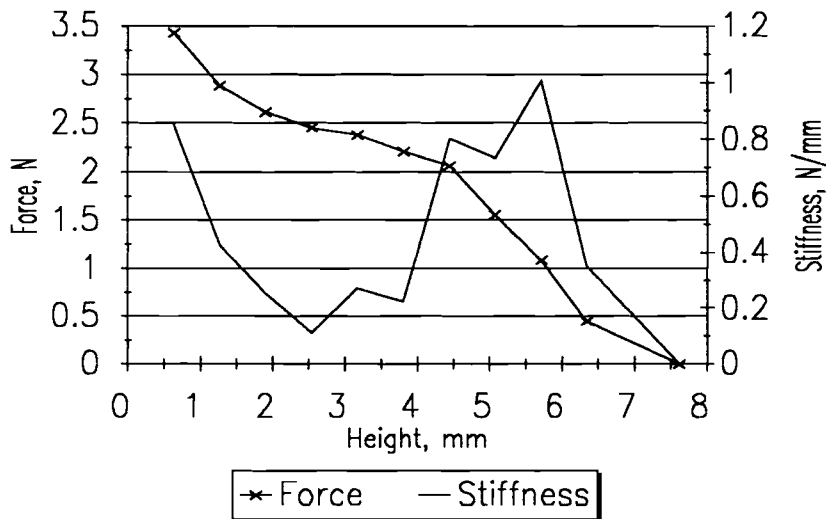


Figure 4.9 Float force for a straight field electromagnetic float polishing apparatus

The design, as developed by Shinmura, is designated as straight field. This is because magnetic field conduction through the polishing chamber is relatively linear from the lower intensifier to the upper intensifier. The force plots for the straight field design show a maximum force when the float is at the bottom of the float chamber, and obtains a value near 3.5 N. This maximum force is of the same order of magnitude as the force developed in the float polishing apparatus done by Tani et al and is not a good comparison to the 7 N that is typical of Umehara and Kato's design.

With the possibility of improving the float force of the electromagnetic polishing apparatus, research has been done with investigation to determine the most advantageous position of the magnetic field intensifiers.

4.4 ANSYS Analysis of Straight Field Electromagnetic Polishing Apparatus

To determine the optimum position of the upper magnetic intensifier and maximum possible buoyant forces, finite element method (FEM) analysis, utilizing the ANSYS package was used to calculate the best position for the upper intensifier.

Figure 4.10 shows the schematic of a straight field electromagnetic apparatus. Initially, ANSYS, a finite element package with electromagnetic analysis capabilities, was used to evaluate the original design. The geometry of the magnetic apparatus is entered into the ANSYS package, generating a drawing of the actual dimensions of the magnetic model.

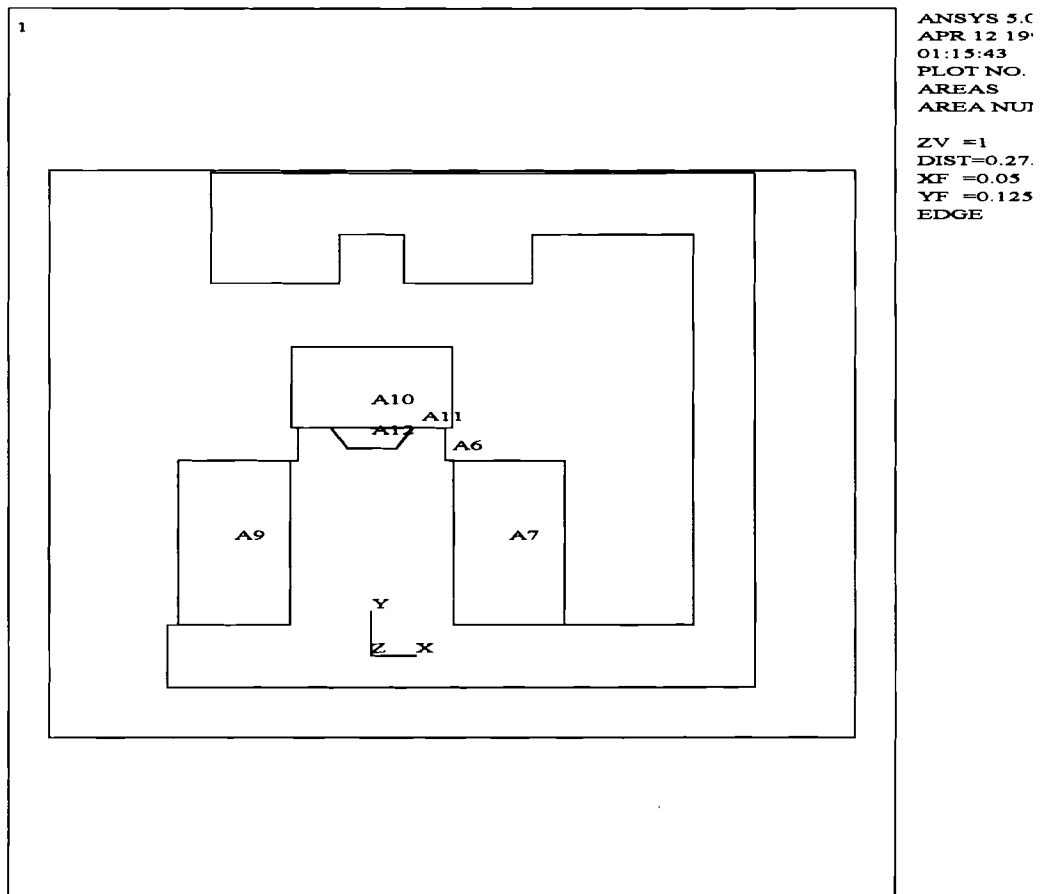


Figure 4.10 ANSYS electromagnetic model for straight field electromagnetic apparatus

This model was generated in the ANSYS program with a script that is given in Appendix B. The title for this particular script is Str_Fld.geo, which represents the straight field geometry portion of the overall model.

Once the model script has generated the model in Figure 4.10, the geometry is meshed using a second script, Str_Fld.mes. This script segments the geometry into different elements that allow ANSYS to determine the magnetic field strength generated by the magnetic coil. To properly model the apparatus the material properties of each component is entered including the permeability of air and steel. The relative permeability of air, which is 1, is specified for all empty areas and for the copper portions of the electromagnetic coil. Figure 4.11 shows the B-H curve for a mild steel. The steel has a specified B-H curve. The material properties are then applied to the steel, copper, and air surrounding the model.

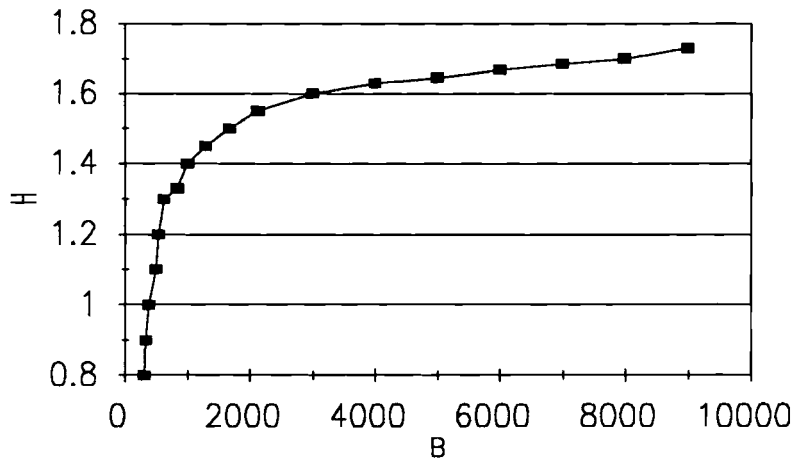


Figure 4.11 B-H curve for mild steel in Tesla

The final stage of the analysis is the calculation of the magnetic field strength. This is accomplished by applying magnetic forces, or body forces, to the two copper coil areas. Since the model is two dimensional, a negative field is applied to the right side of the magnetic coil and a positive field to the left side. This generates a two dimensional

analysis of circular magnetic coil, generating a magnetic field lengthwise along the steel core. The ANSYS model is solved according to the solution script provided in Appendix B and the model can then be viewed.

Figure 4.12 is a plot showing the variation of magnetic field B , and Figure 4.13 shows variation of H , for the straight field model. Generalizations can be made about the buoyant force inside the polishing chamber from reviewing the intensity of the magnetic field in the polishing chamber area. Even though the buoyant force is relative to the magnetic field gradients, the magnetic field intensity is a good indication of the possible gradients in the area.

Using ANSYS we can calculate the theoretical magnetic field strength in each of the elements generated during the analysis. These magnetic field strengths can then be stored in a file and later incorporated into a spreadsheet that allows the manipulation and alteration of the magnetic field strengths and gradients into force plots that can be utilized for design purposes. The data used in this analysis is extracted from the ANSYS data by incorporating an area of specified element dimensions. A plot of the magnetic field strength for the area of interest, inside the polishing chamber, is shown in Figure 4.14. It shows the theoretical calculation of B for a specified geometry, magnetic coil current, and intensifier design.

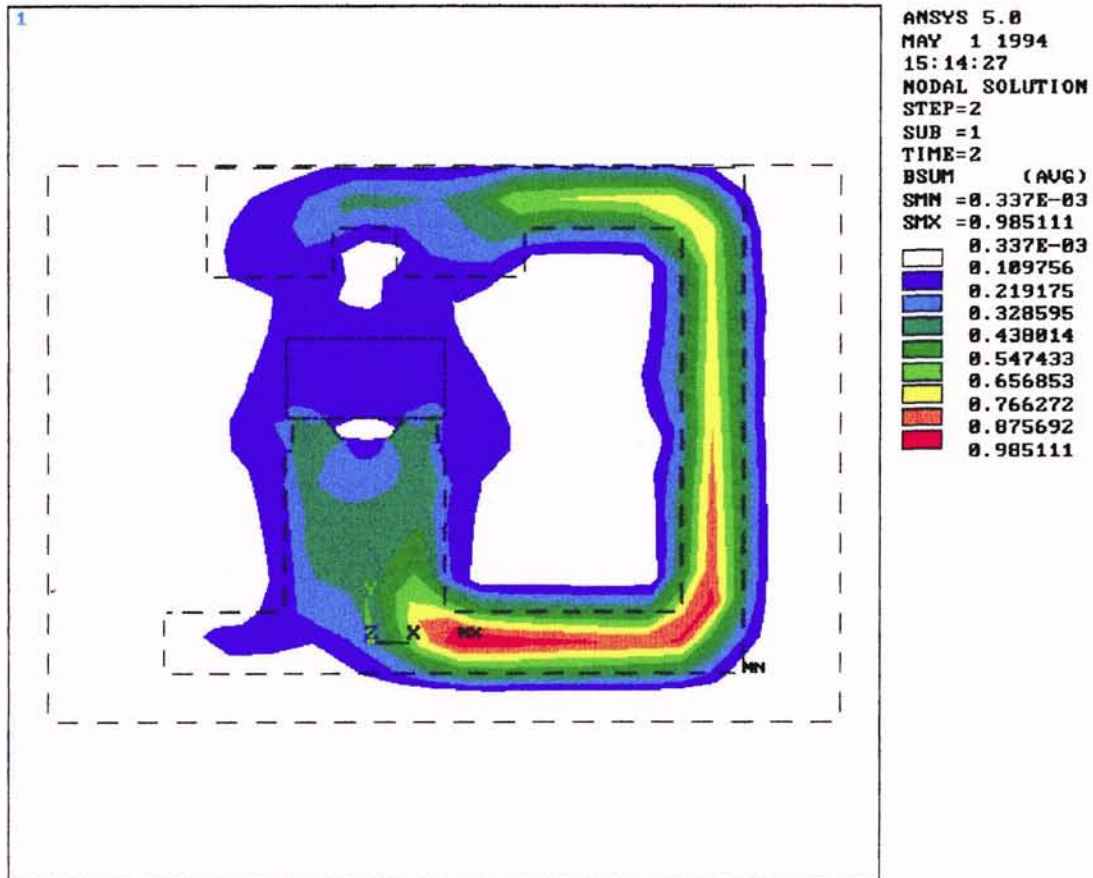


Figure 4.12 B for straight field electromagnetic float polishing apparatus

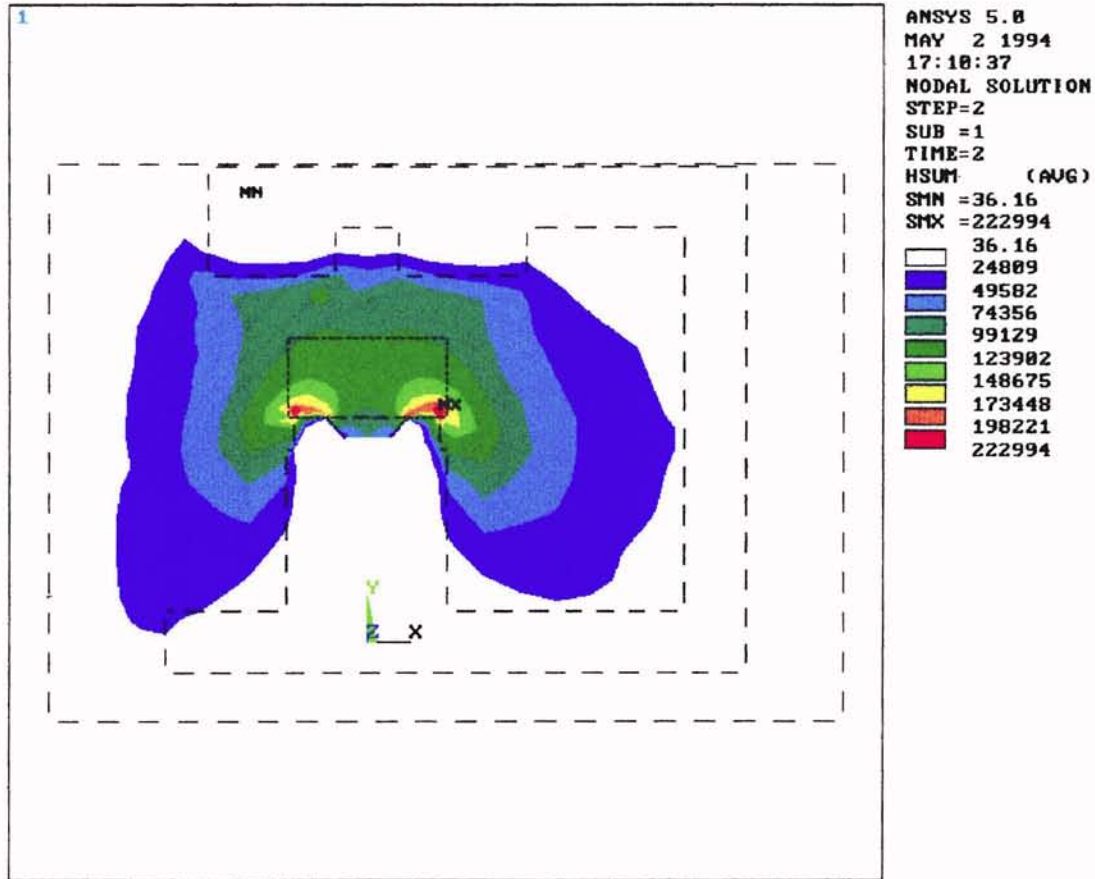


Figure 4.13 H for straight field electromagnetic float polishing apparatus

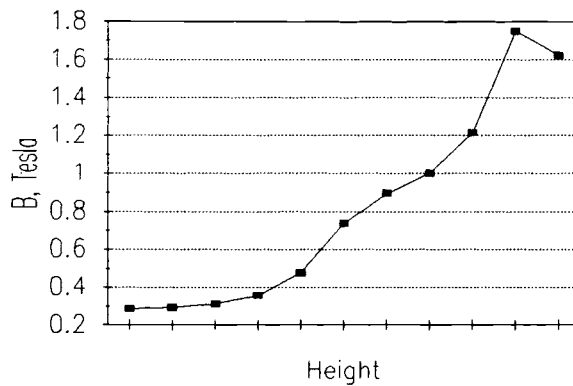


Figure 4.14 B versus height for straight field electromagnetic apparatus

Typically ANSYS generates elements inside the model by utilizing varying geometries that best fit the required element size. For this reason, the elements can be four and three sided, and often vary in size and shape. To extract the required information from the finite element, area of specified shape and size elements are generated in the area that determines the buoyant forces of the float polishing. These elements are the extracted field strengths used to determine the float forces. The elements are square and of equal size to allow detailed determination of the magnetic field strengths and the gradients involved in float polishing.

The magnetic field strength for the ANSYS model is generated by applying a body force to the magnetic core of the electromagnetic model. The body force, as termed by ANSYS, is the current per area in the model. The current per area for the magnetic coil used in the electromagnetic model is determined by the Amp-turns of magnetic wire, 3 Amps and 5400 turns of wire. This yields 16200 Amp-turns of wire, with a 3 in by 5 in area (magnetic coil). This yields around $1.5 \times 10^6 \text{ A/m}^2$ of applied body force.

After solving the model in ANSYS the field strength above the lower intensifier can be

extracted from the finite element analysis program. Figure 4.15 shows buoyancy force determined from calculation using the ANSYS data. The program used to determine this buoyant force is given in Appendix C. This program generates the buoyancy force, assuming magnetic fluid strength and float thickness.

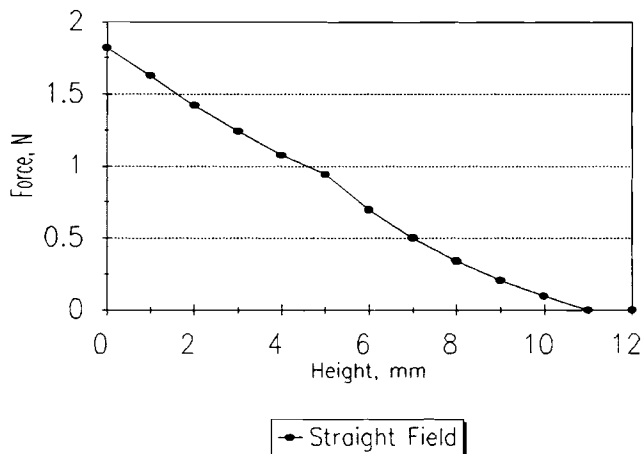


Figure 4.15 Variation of theoretical buoyancy force with height for straight field electromagnetic apparatus using ANSYS simulation.

This theoretical float force, of almost 2 N, is slightly lower than the experimental float force of 3.5 N. However, these variations can be accounted for in the variances associated with the different types of magnetic fluid, varying float densities, and discretization of the theoretical model. The theoretical model does show that the float forces will be substantially lower than forces experienced by Umehara and Kato (1990).

The solution to the lower float forces is to redesign the straight field electromagnetic machine to have higher field strengths and higher magnetic gradients causing higher float forces. To increase the magnetic field strength and the gradient, the position of the upper intensifier must be lowered, i.e. a closer lower intensifier, causing a shorter magnetic field path. This is accomplished by modifying the apparatus into a ring pole.

4.5 ANSYS Analysis of Ring Pole Electromagnetic Polishing Apparatus

Modifications to the electromagnetic float polishing apparatus has been made to generate higher field strength and higher gradients than that experienced in the original design (straight field). This design was determined by realizing that the field strength through the polishing chamber increases as the gap between the lower and upper intensifier decreases. The limit to this lowering of the upper intensifier is the ring pole design.

As the intensifier lowers to the point that it contacts the polishing chamber, it must be enlarged to wrap around the polishing chamber as a magnetic ring. The ring pole can then be lowered further to completely surround the polishing chamber. Figure 4.16 shows a schematic of the ring pole design when a ring envelopes the circumference of the float chamber.

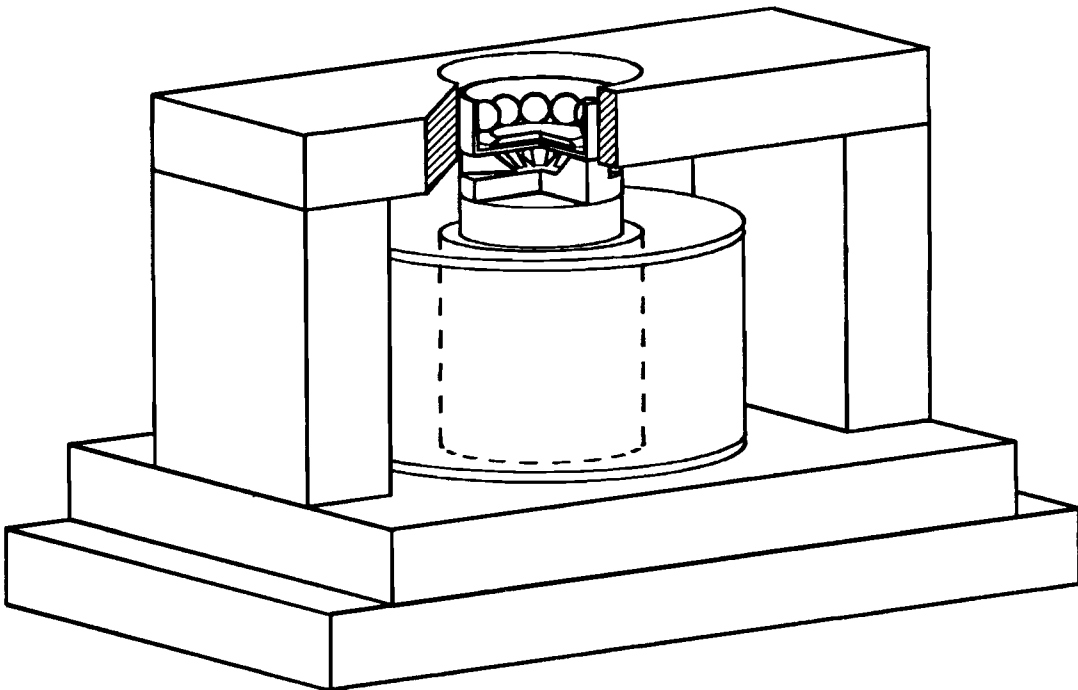


Figure 4.16 Ring pole electromagnetic float polishing apparatus

The ring pole design is idealized by two conductors approaching the center core from each side. This geometry approximates the actual geometry of a circular ring around the

central magnetic core. Figure 4.17 shows ANSYS model of the ring pole design.

The ring pole model was analyzed in ANSYS starting with a script file (for details see Appendix B, titled ring_0.geo). The model was then meshed, with script ring_0.mes, and solved with the same magnetic field strength and material properties as the straight field model. The solution script for the ring pole case is shown in Appendix B under ring_0.sol.

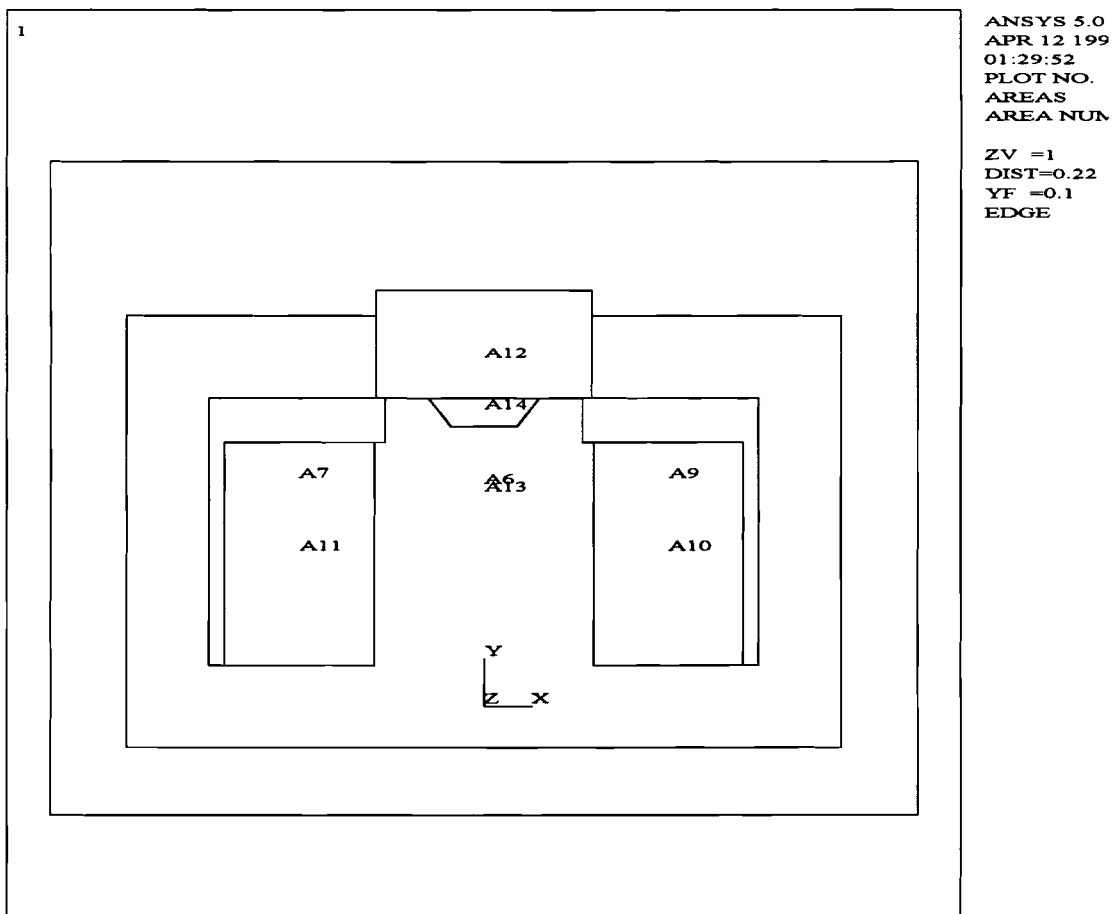


Figure 4.17 ANSYS model for ring the pole apparatus.

The B and H plots for the ring pole are shown in Figures 4.18 and 4.19 respectively. B shows the “current” generated by the magnetic field and the loss of this magnetic field strength throughout the polishing apparatus, while H shows the regions of magnetic

central magnetic core. Figure 4.17 shows ANSYS model of the ring pole design.

The ring pole model was analyzed in ANSYS starting with a script file (for details see Appendix B, titled ring_0.geo). The model was then meshed, with script ring_0.mes, and solved with the same magnetic field strength and material properties as the straight field model. The solution script for the ring pole case is shown in Appendix B under ring_0.sol.

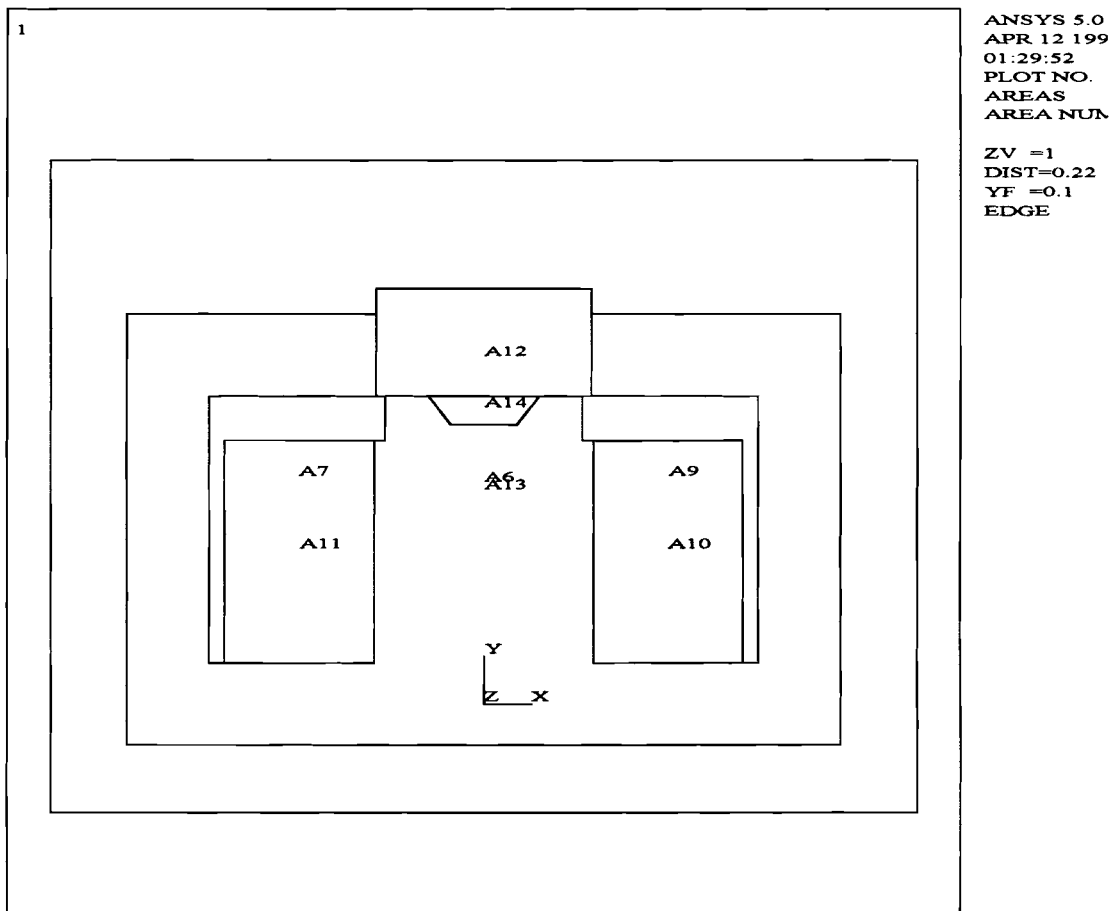


Figure 4.17 ANSYS model for ring the pole apparatus.

The B and H plots for the ring pole are shown in Figures 4.18 and 4.19 respectively. B shows the “current” generated by the magnetic field and the loss of this magnetic field strength throughout the polishing apparatus, while H shows the regions of magnetic

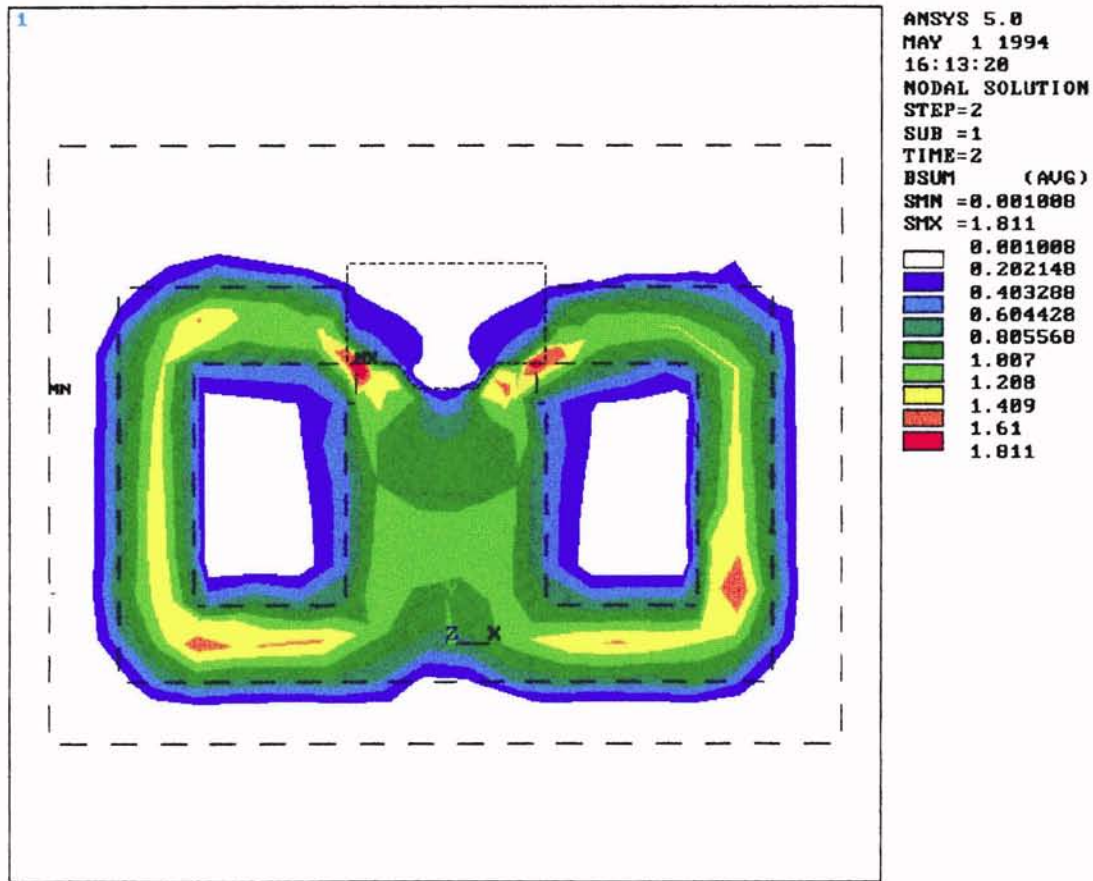


Figure 4.18 B plot for ring pole electromagnetic apparatus

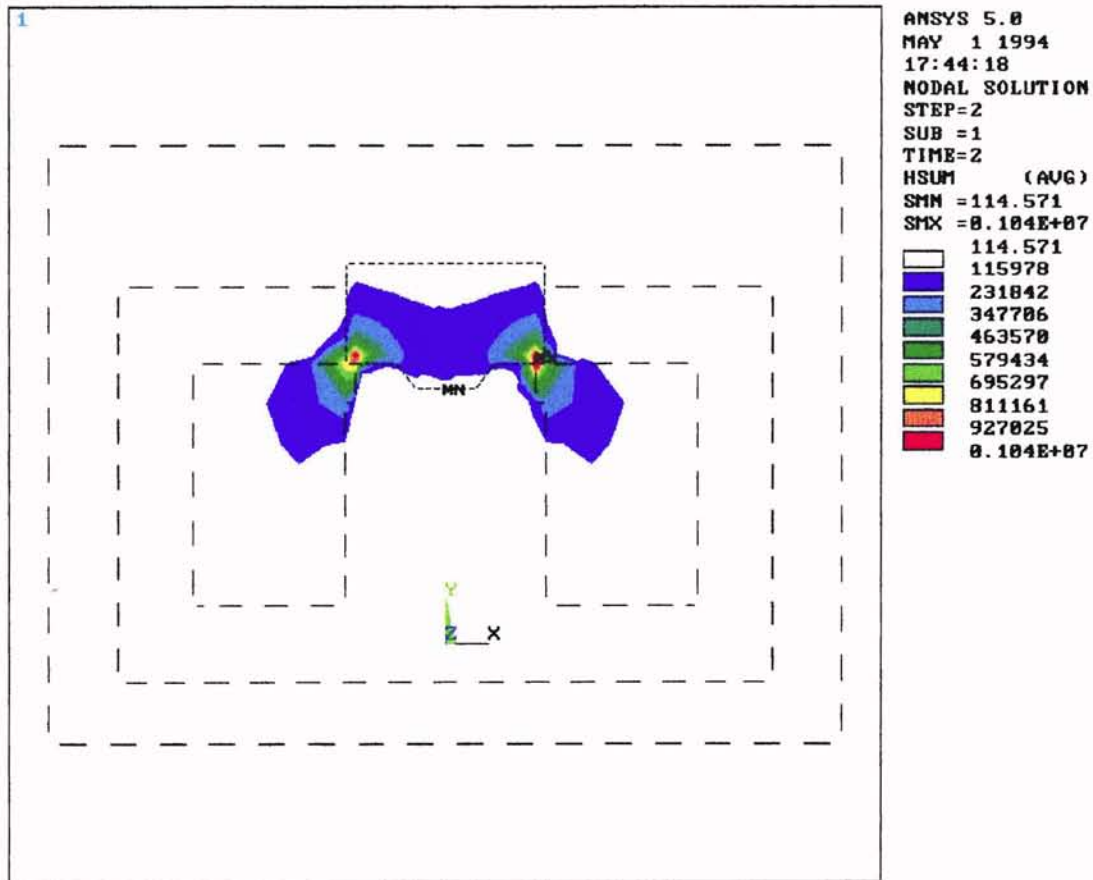


Figure 4.19 H plot for ring pole electromagnetic apparatus

field loss.

A comparison of the straight field and ring pole analysis shows the differences between the geometry of two designs in the available field strength and gradients. For the ring pole case ANSYS analysis was done with varying gaps between the bottom of the ring pole and the lower intensifier. The gap between the bottom of the ring pole and the lower intensifier is important because of its influence on the magnetic field conduction, magnetic field gradients, and polishing attributes. Figure 4.20 shows a geometric representation of the gap between a ring pole and the lower intensifier for clarity.

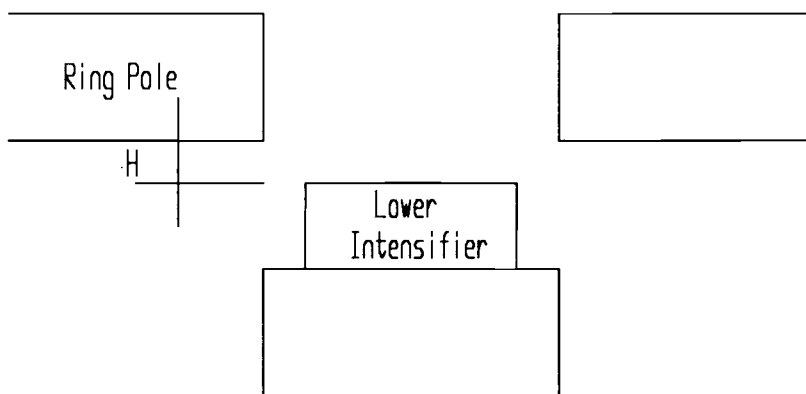


Figure 4.20 Geometric representation of the gap between the ring pole and the lower intensifier

Figure 4.21 shows the field strength, B , for straight field, 6 mm ring pole height, and 10 mm ring pole height to demonstrate the magnetic field improvement with the alteration to float polishing apparatus.

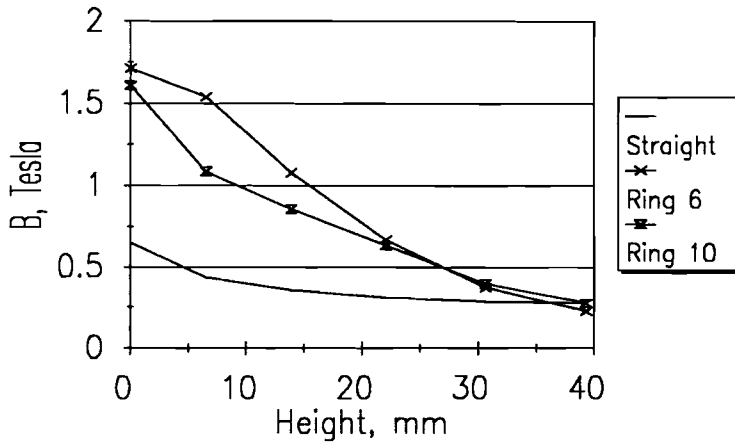


Figure 4.21 Field strength for straight field and ring pole designs

The values of 6 mm and 10 mm represent the height of the ring pole above the field intensifier (see Figure 4.20). It should be noted that a ring pole system of 6 mm height had the highest field strength relative to 10 mm height ring pole system and straight field system due to the higher conductance of the magnetic field through the polishing apparatus.

From Figure 4.22 shows the variation of buoyant force with height for straight field, 0 and 3 mm, it can be seen that the force of the straight field system about 3 N and gradually increasing toward the bottom of the polishing chamber. The two ring pole designs, zero height ring pole and 3 mm high ring pole, show much higher forces than the straight field, but force vs. height shapes are different than the straight field case. The ring pole design [3 mm] has an increasing force to the depth of the ring pole gap, then a decrease in buoyant force followed by an increase in force to the bottom of the polishing chamber.

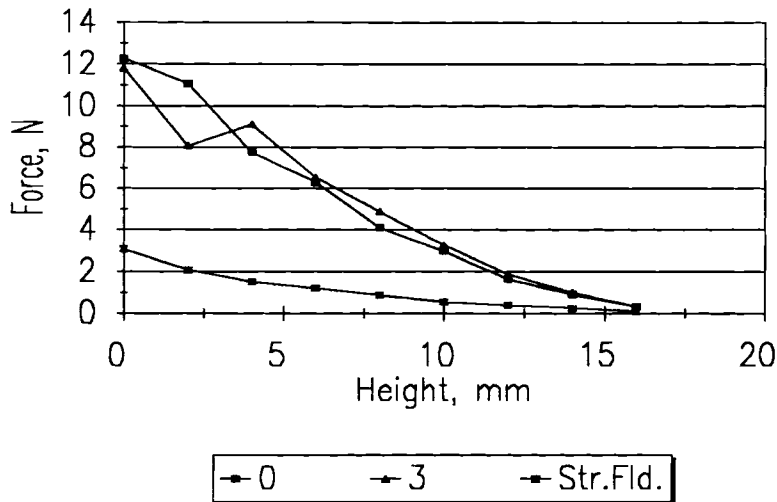


Figure 4.22 Force versus height, h , for the ring pole and the straight field designs

The results of this force decrease at a float height equal to the ring pole gap is a region of negative stiffness. Experimentally this phenomenon occurs when the ring pole gap is larger than 6 mm. With this size gap a 5 mm ball is pushed to the bottom of the polishing chamber where it will remain until lifted. A negative stiffness in float polishing can result in increasing sphericity due to lower forces at large diameters. The negative stiffness in this region would polish larger diameters less, and previously polished (smaller regions) balls would receive excess material removal resulting in a deterioration in the sphericity of the ceramic ball.

Therefore, for the purpose of float polishing of ceramic balls for bearing applications requiring adequate sphericity, the ring pole design with zero intensifier gap shows the most promise for an efficient and geometrically acceptable polishing process. The straight field design shows insufficient buoyant forces, and the ring pole designs with gaps between the ring pole and the lower intensifier show negative stiffness inside the polishing chamber which would adversely affect the sphericity of the polished ball.

4.6 Experimental Evaluation of Forces in the Ring Pole Designs

To determine the effectiveness of the ANSYS analysis, comparisons have been made between the theoretical and experimental buoyant forces. Initially, the theoretical data is modified to approximate the experimental conditions of the actual polishing apparatus. The buoyant forces shown in Figure 4.23 are averaged over 6 mm which is the thickness of a typical float. This averaging accounts for the buoyant forces at the bottom, middle, and top of the actual float of 6 mm thickness.

Another modification to the theoretical data is accountability for the limited ferrofluid volume. Theoretical buoyant forces do not account for the limited depth of the ferrofluid inside the polishing chamber resulting in buoyant forces above 10 mm of float depth. However, buoyant force experiments rarely generate forces above 10 mm because of the limited depth of the fluid inside the float chamber. For this reason the buoyant forces are proportionally decreased between 5 mm and 11 mm to approximate the 6 mm thick float rising from the surface of the fluid. At a float depth of 5 mm, the float is fully submerged and exposed to the full buoyant force of the ferrofluid. Likewise, at 11 mm the float is completely buoyant at the surface of the fluid and cannot generate any external force. The comparison shows the assistance of the ANSYS model in predicting the forces possible in magnetic fluid polishing.

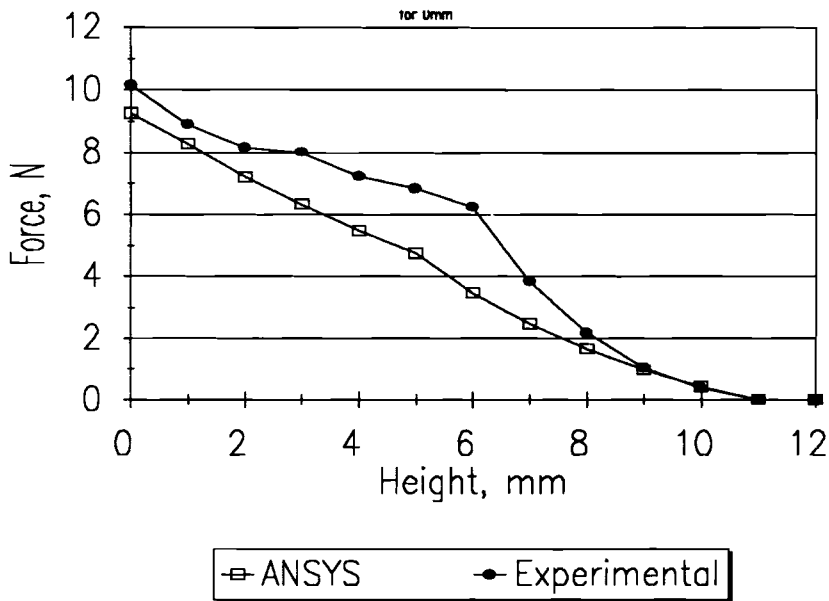


Figure 4.23 Experimental and theoretical values for electromagnetic float polishing.

The ANSYS analysis has the ability to determine the float polishing characteristics before construction of a specified geometry. The theoretical and experimental float forces for the zero height ring pole design are within acceptable variance. The ANSYS analysis also predicted problems with negative stiffness in any situation where a gap between the ring pole and the lower field intensifier is allowed. The minimization of this gap, along with high field strength allowed ANSYS to predict good buoyancy forces without negative stiffness.

CHAPTER 5
DESIGN OF EXPERIMENTAL APPARATUS

5.1 Evaluation of Polishing with the Ring Pole Design

Once the ring pole design had been analyzed and optimized, experiments were performed to determine if the ANSYS evaluation of the ring pole design was adequate. Certain assumptions were made in the ANSYS analysis, such as a two dimensional design with a donut shaped field intensifier that might alter the true polishing characteristics of the apparatus. A polishing experiment was performed with 10.3 mm silicon nitride ceramic balls polished with 10 volume percent silicon carbide utilizing a nylon bottom float plate. The results of this experiment are shown in Figure 5.1.

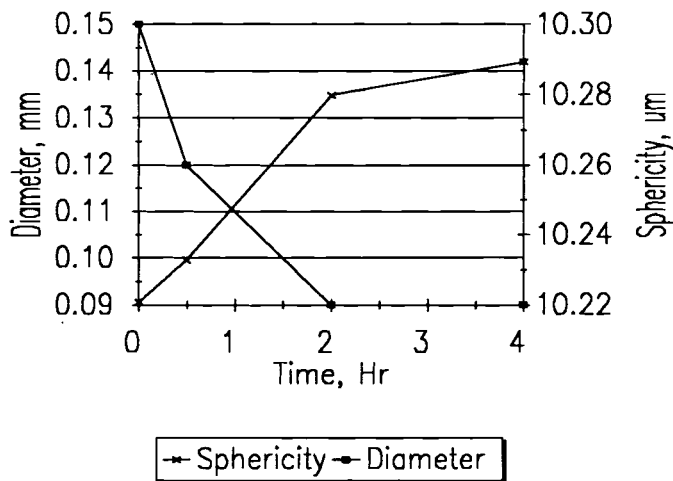


Figure 5.1 Results of electromagnetic float polishing with convoluted intensifier

The results of the experiment given in Figure 5.1 show an increasing error in form. The sphericity of the ball is continually increasing lowering the quality of the produced ceramic ball element. The cause for the increasing sphericity is found to be the lower magnetic intensifier, originally developed to increase the float forces during polishing.

5.2 Convoluted Magnetic Field Intensifier

The problem with a convoluted magnetic field intensifier is the varying magnetic field strength which leaves weak magnetic field strength and lower magnetic field gradients between the protrusions of the intensifier. This imparts both positive and negative forces on the ceramic ball causing poor sphericity. Figure 5.2 represents a magnetic field intensifier with convolutions and its effect on the buoyancy force. The solution to this problem is to remove the cutouts in the intensifier and have a “donut” shaped intensifier that lacks the field inversions that are associated with the convoluted intensifier.

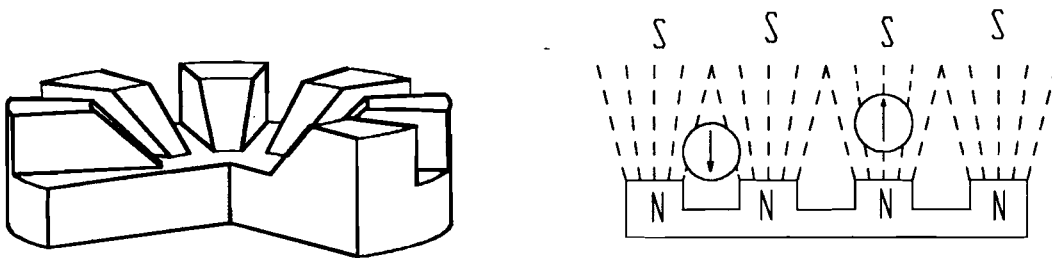


Figure 5.2 Magnetic field lines for a convoluted magnetic field intensifier

This convoluted magnetic field intensifier is similar to a ring pole design with a gap between the bottom of the ring pole and the upper field intensifier. The extra distance between the ring pole and the intensifier causes a region of negative stiffness which will hold the ball away from the top plate, responsible for polishing. This is corrected with a non-convoluted magnetic field intensifier as shown in Figure 5.3.

5.3 Design Modification for Removal of Excessive Heat

During initial polishing experiments it was found that the heat generation by the magnetic coil and the heat from material removal processes tend to evaporate the water

based magnetic fluid. This reduction in magnetic fluid causes an increase in the viscosity of the fluid in the polishing chamber which lowers the mobility of the ceramic balls during polishing. For this reason, a water cooling system was incorporated into the magnetic field intensifier to lower the operating temperature of the polishing chamber. Figure 5.3 shows the result of altering the field intensifier for improved magnetic field shape and reduced heat conduction to the polishing chamber. The temperature of the polishing chamber was dropped from 100° F to under 80° F allowing longer polishing times with less viscosity increase.

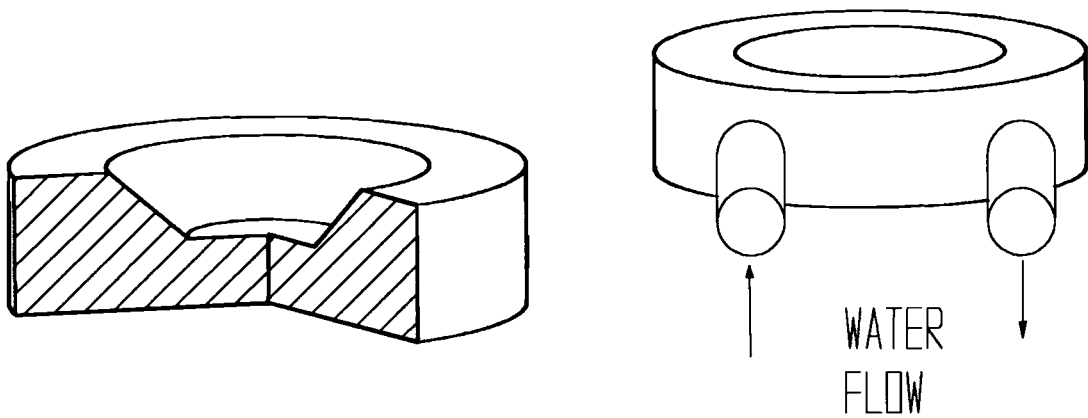


Figure 5.3 Upgraded magnetic field intensifier with water cooling system.

CHAPTER 6
EXPERIMENTAL PROCEDURES
AND TEST RESULTS

6.1 Experimental Procedure

Experiments performed for the determination of polishing characteristics were standardized to maintain consistency during experimentation. A standard procedure was developed to determine the characteristics of the ball element. Table 6.1 lists attributes of ceramic ball elements that are characterized.

Table 6.1 Attributes of ceramic balls for bearing applications

Diameter	Δ Diameter	Sphericity	Surface Roughness, R_{max}
5 mm	0.1 μ m	0.1 μ m	5 nm - 10 μ m
- 12 mm	-100 μ m	-100 μ m	

These attributes are measured before and after each experiment to determine the effect of a particular experimental sequence. The diameter is measured with a digital micrometer and has been found to be accurate within $\pm 3 \mu$ m. The Δ Diameter parameter is the difference between the maximum and the minimum diameter values, and is derived from the diameter measurements. The sphericity is determined with a TalyRond measuring apparatus. The resolution of the TalyRond is $\pm .05 \mu$ m and determines the roundness of the ball for every point around ball, unlike Δ Diameter which is calculated from a few discrete points. The Δ Diameter value and sphericity are closely related but differ in the calculation technique.

The surface finish is measured with a TalySurf machine. A typical set of data, for a CERBEC (NBD 100) finished ball is shown in Table 6.2. This data is used for comparison between conventionally finished ceramic balls and magnetic float polished balls.

Table 6.2 Data for Cerbic ceramic ball

Cerbec Base line data from polished Cerbec ceramic balls

Ball No.	1	2	3	4	5	6	7	8	
1	7.942	7.945	7.942	7.943	7.942	7.943	7.940	7.940	Dimensions in mm
2	7.941	7.944	7.941	7.942	7.941	7.941	7.942	7.942	
3	7.941	7.943	7.942	7.942	7.941	7.942	7.942	7.942	
4	7.942	7.942	7.944	7.942	7.941	7.945	7.942	7.942	
5	7.941	7.942	7.941	7.942	7.941	7.942	7.941	7.942	
6	7.945	7.942	7.941	7.941	7.941	7.941	7.942	7.942	
7	7.944	7.942	7.941	7.942	7.940	7.942	7.943	7.943	
8	7.944	7.942	7.942	7.941	7.941	7.944	7.941	7.942	
9	7.945	7.942	7.941	7.941	7.942	7.943	7.941	7.943	
10	7.945	7.942	7.941	7.941	7.942	7.944	7.940	7.943	
AVG	7.943	7.943	7.942	7.942	7.941	7.943	7.941	7.942	AVG (Total)
Avg Std	0.004	0.003	0.003	0.002	0.002	0.004	0.003	0.003	0.003
Avg Std	0.002	0.001	0.001	0.001	0.001	0.001	0.001	0.001	0.001

AVG Average of data values
 Maximum - Minimum diameter value
 Avg Std Standard Deviation of data values

The data in Table 6.2 is representative of data taken for all experiments during the research into the effects of electromagnetic float polishing. Along with Talysurf surface finish and Talyrond sphericity, the diameter data determines the changes in the ball characteristics during polishing.

6.2 Variables Involved in Electromagnetic Float Polishing

Under consideration during polishing of ceramic ball elements are the variables determined by Umehara and Kato (1990) to be of significance relative to the polishing process. Table 6.3 shows a listing of the variables involved during the float polishing process.

Table 6.3 Variables involved in electromagnetic float polishing

Rotational Speed	1000 rpm - 20000 rpm
Grinding Load	1 N - 15 N
Abrasive Concentration	1 % - 20 %
Grain Size	up to 200 μm
Abrasive Type	B ₄ C, SiC, and Cr ₂ O ₃
Abrasive Hardness, kg/mm ²	B ₄ C 2800, SiC 2500, and Cr ₂ O ₃ 1250

The rotational speed, grain size, and abrasive type have been studied to determine correlation between electromagnetic float polishing and permanent magnet float polishing.

6.3 Electromagnetic Apparatus Polishing Results

Results from polishing tests with the electromagnetic float polishing machine have shown that the process can be expected to produce quality ceramic components quickly and efficiently. The initial results with the ring pole system, and updated field intensifier, are shown in Figure 6.1.

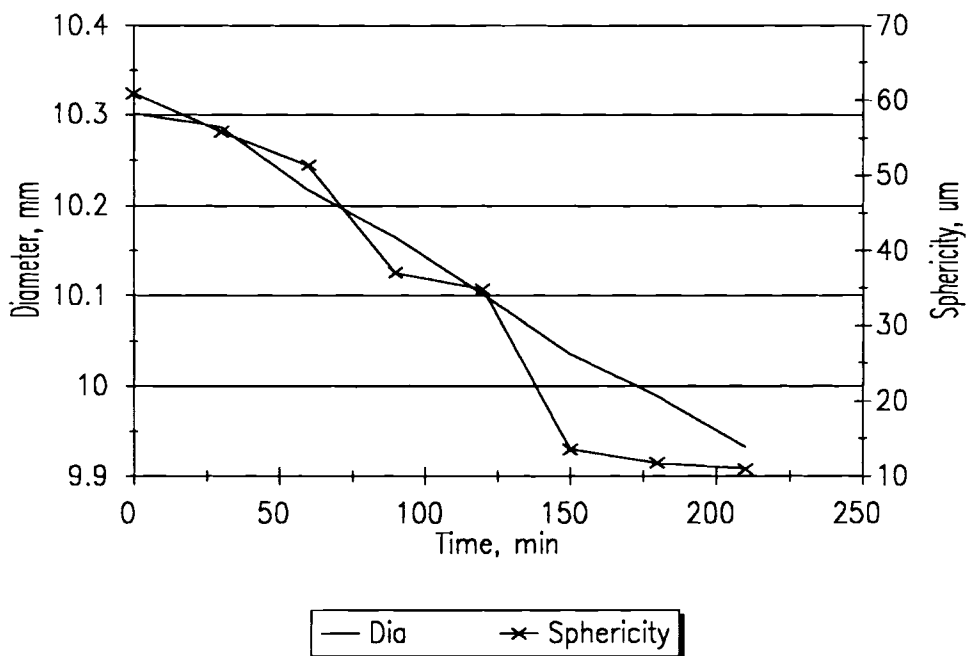


Figure 6.1 Diameter and sphericity variation of Si_3N_4 balls using an electromagnetic polishing apparatus.

From Figure 6.1, it can be seen that the diameter decreases with time, i.e. gradual negative slope with consistent material removal and more importantly the sphericity of this specimen dropped from 60 μm to 10 μm , which is an excellent improvement compared

to previous experiments which yielded an increasing sphericity. The following experiments show the relationships of material removal rate against the removal rate, abrasive type, and abrasive size.

6.4 Effect of Revolution Speed on Material Removal

Figure 6.2 shows the results of this polishing experiment. The effect of rotational speed on material removal rate was determined in the electromagnetic float polishing apparatus with full magnetic field (near 1.6 T) a 12.5 mm nylon float plate, air bearing spindle, and 10 volume percent of boron carbide (B_4C). The balls were polished with a Professional Instruments air bearing spindle capable of 10000 rpm. This particular experiment is for 2000 to 8000 rpm.

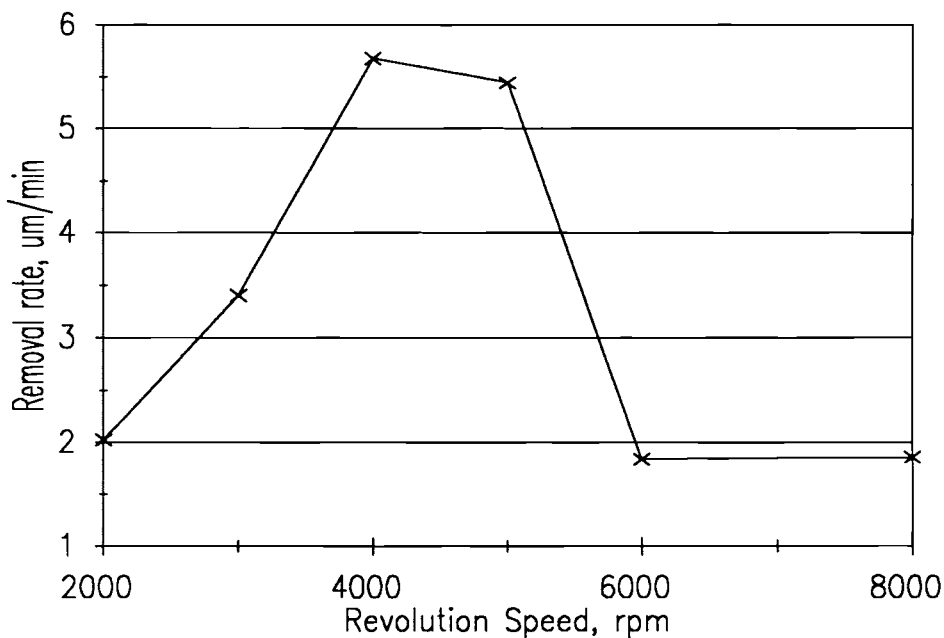


Figure 6.2 The relationship between removal rate and revolution speed

There is an increase in material removal, from 2000 rpm, with increasing rotational speed up to an optimum speed followed by a reduction in the material removal rate with further increase in speed. The drastic drop is probably due to instability in the polishing chamber, which was evident from an increase in vibration (noise) during polishing at

the higher speeds. Other experiments, with different geometries and abrasive, show a similar trend with a different transition speed.

6.5 Effect of Abrasive Grain Type on Material Removal

Figure 6.2 shows the effect of abrasive grain type on material removal rate. The abrasive grains utilized in these experiments include B_4C , SiC , and Cr_2O_3 . The abrasive grains were all utilized at 10 volume percent in the magnetic fluid. The abrasive grains are 500 grit B_4C , 400 grit SiC , and 1200 grit Cr_2O_3 .

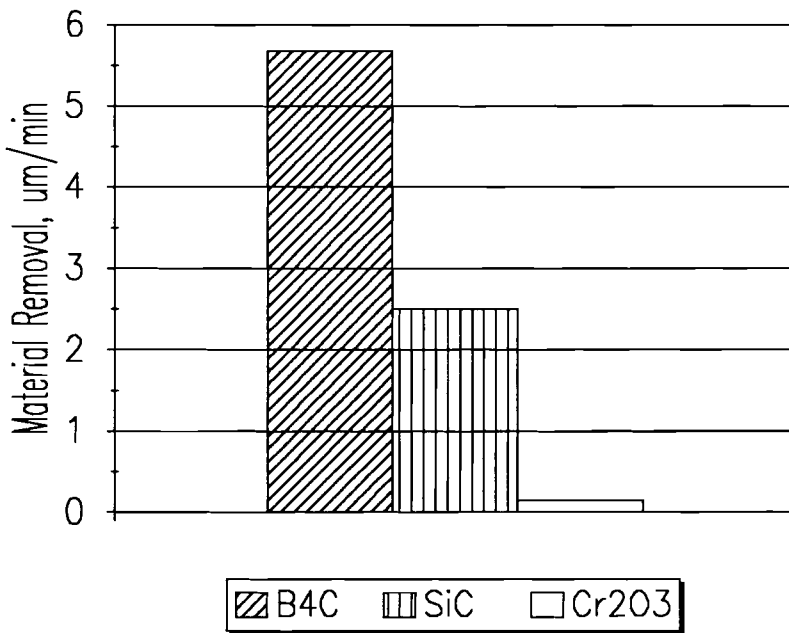


Figure 6.3 Effect of abrasive type on material removal rate.

6.6 Effect of Abrasive Size on Material Removal

Of more importance to removal rate for a given abrasive is the effect of abrasive grain size. For the three separate abrasive different grain sizes were used to determine the material removal versus grain size.

Three grain sizes were used with boron carbide. Experiments were performed with 500,

800, and 1500 grit boron carbide, 400, 600, and 100 grit silicon carbide, and 1200 grit chromium oxide. Figure 6.4 shows the results of these experiments, smoothed with a quadratic approximation.

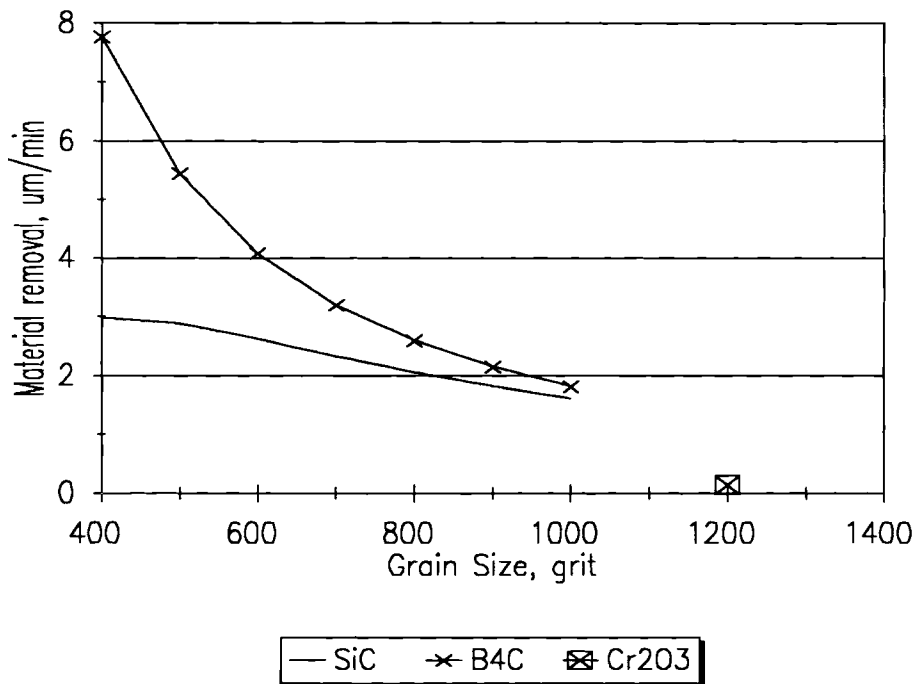


Figure 6.4 The relationship between material removal rate and grain size

While both silicon carbide and boron carbide have approximately the same material removal below 1000 grit, the effect of the abrasive at a larger diameter is apparent. The boron carbide abrasive has a higher removal rate when rough polishing due to its higher hardness over silicon carbide.

6.7 Effect of Abrasive Grains on Surface Roughness

The surface roughness for the ceramic ball bearings is determined by the abrasive type and grain size used during the polishing process. Table 6.3 shows the relationship between the abrasive size and type and this effect on the final surface finish.

Table 6.4 Effect of abrasive type and size on final surface finish

Type	Size	Roughness, R_{max} , μm
B_4C	500	1.075
B_4C	800	0.947
B_4C	1500	0.536
SiC	400	1.448
SiC	600	1.142
SiC	1000	0.723
Cr_2O_3	1200	0.171

6.8 Control of Sphericity

The sphericity of the silicon nitride ball elements is lowered during polishing with the electromagnetic float polishing apparatus. The sphericity of a ceramic ball, during polishing with silicon carbide, is shown in Figure 6.5. The sphericity is shown to initially drop then rise. During this rise period it was found that excessive heat vaporized the magnetic fluid causing the abrasive grains and balls to run dry inside the polishing chamber. The lack of fluid inside the polishing chamber caused an increase in sphericity which was later corrected with improved cooling techniques, i.e. addition of water cooling system to the electromagnetic apparatus.

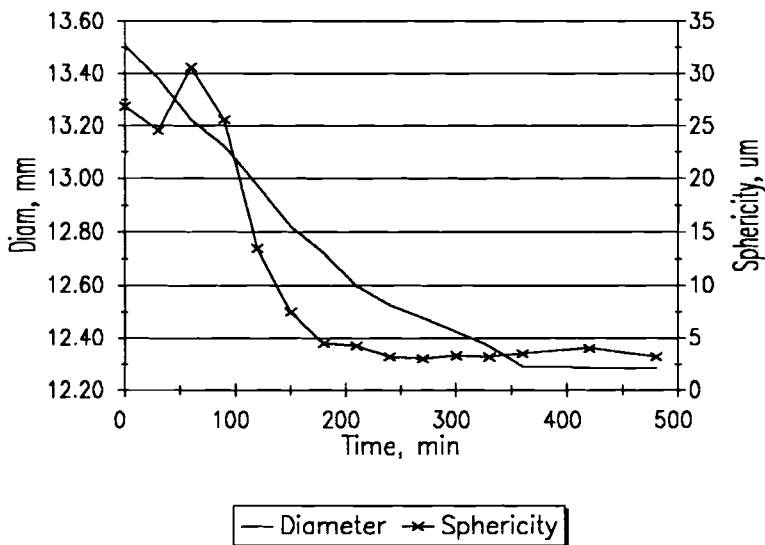
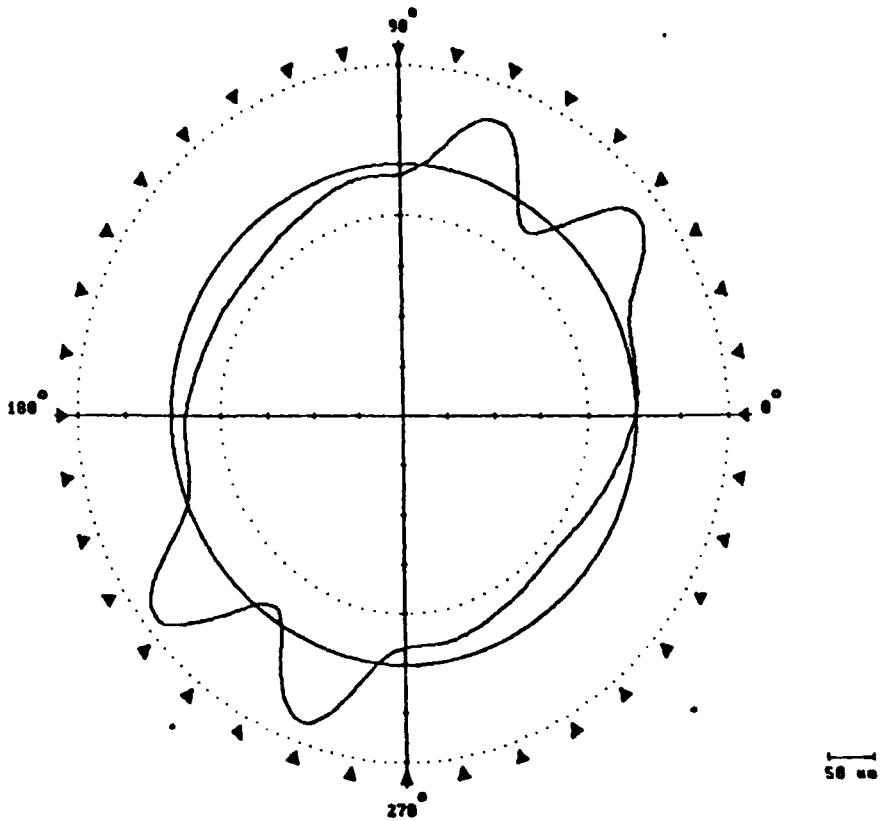


Figure 6.5 Variation of diameter and sphericity with time for electromagnetic float polishing

An initial sphericity and final sphericity from electromagnetic float polishing is shown in Figures 6.6 and 6.7. The original sphericity is due to the surface permutation left during the hip process, which yields a 123.25 μm sphericity. The final sphericity, for this experiment, is 2.90 μm and the 3 lobe geometry of the float polished ball is evident.

USU Mechanical Engineering

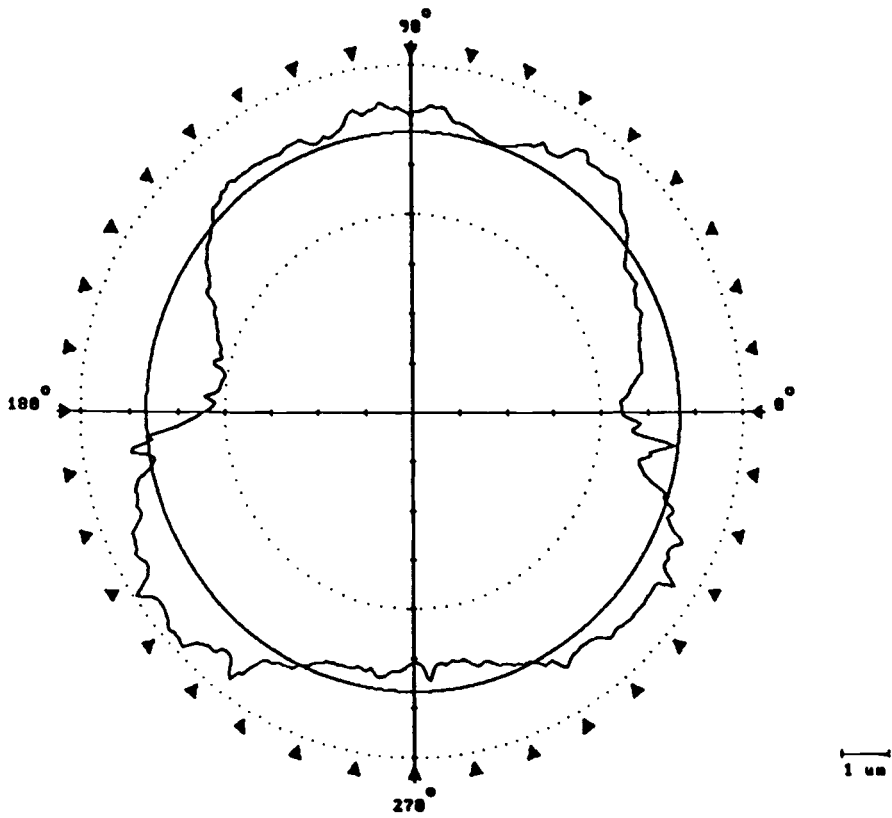
Date 14-11-94 11:59
 Feature DFAULT 00



LS ROUNDNESS RESULTS

○	123.25 um	Mean. mode	External
E	34.95 um	Z Height	150.0 um
∠	281.0 deg	Filter	50 upr 2CB
↗	174.60 um	Profile	100.0 X
.	Datum : SPINDLE		

Figure 6.6 Initial sphericity of a silicon nitride ceramic ball



LS ROUNDNESS RESULTS

○	2.98 μm	Meas. mode	External
E	16.45 μm	Z Height	149.6 μm
∠	21.3 deg	Filter	50 upr 2CR
↗	32.60 μm	Profile	100.0 X

Datum : SPINDLE

Figure 6.7 Final sphericity of a polished silicon nitride ball

CHAPTER 7

DISCUSSION

7.1 Construction of Electromagnetic Apparatus

The electromagnetic polishing apparatus was built using the design developed by Dr. Shinmura of Japan. The design drawings were redrawn in CADKEY. The apparatus was built on the Bridgeport machine tool with standard construction techniques. While the construction of the apparatus was not difficult the possibility of improving the electromagnetic apparatus was made possible due to the ANSYS analysis software which became available subsequent to the construction of the apparatus.

Analysis of the apparatus with ANSYS proved invaluable to optimizing the electromagnetic float polishing apparatus without multiple construction iterations that would have normally occurred. ANSYS accurately predicted that a ring pole design would yield higher buoyancy forces, but a gap between the ring pole and lower intensifier would cause negative stiffness values in the force versus height plot. This negative stiffness became apparent when polishing with the convoluted lower intensifier due to the cutouts in the intensifier acting as a gap between the intensifier and the ring pole. Initial experiments evaluated the performance of the electromagnetic machine and negative stiffness caused an increasing sphericity in the ceramic ball. This increasing sphericity was later corrected with an improved lower intensifier.

With corrections made to the intensifier and improved magnetic field strength, the electromagnetic apparatus has shown promise for polishing ceramic components. The equipment has given higher float forces than Umehara's equipment, 7 N for Umehara and 10 N for the electromagnetic equipment, with comparable material removal rates.

The electromagnetic apparatus also has a modified bouyant force versus height plot that allows lower stiffness at higher forces which may allow improved surface finish capabilities.

7.2 Polishing Experiments

The polishing experiments performed to determine the characteristics of the polishing apparatus have shown the possibilities of competing with permanent magnet apparatus. The electromagnetic apparatus has force controllability unlike a permanent magnet apparatus. The electromagnetic apparatus can alter the magnetic field strength during the polishing process allowing high initial forces for material removal, then reduced forces to minimize surface damage during the finishing process.

Results from the material removal rate versus rotational speed of the spindle show room for improvement with geometry inside the float chamber. The polishing apparatus, at higher speeds, show signs of vibrational instability due to geometry peculiarities in the lower float.

The material removal versus abrasive type showed the benefits of hard, and soft abrasive grains. Hard abrasives, such as B_4C have a higher material removal rates for a given grain size. The softer abrasive grains, namely Cr_2O_3 , do not remove material as well, but the minimum obtainable surface roughness, R_{max} , shows the advantage of removing material with soft abrasive grits.

The sphericity of the ceramic ball elements was found to decrease with time to a minimum value, and then maintain a constant value regardless of alterations to the system. Varying float material with nylon, plexiglass, aluminum, and stainless steel had little effect on the minimum obtainable sphericity.

CHAPTER 8

CONCLUSIONS AND FUTURE WORK

8.1 Summary of Present Work

An electromagnetic apparatus was constructed to develop the expanding possibilities of magnetic float polishing. The equipment was designed by Dr. Shinmura of Japan, and drawings were stored in CADKEY software package.

Dr. Shinmura's original design achieved float forces of approximately 3.5 N, which is lower than that of a permanent magnet apparatus of 7 N. For this reason, ANSYS magnetic analysis was performed to determine the optimum geometry of the electromagnetic apparatus. The revised design, ring pole electromagnetic float polishing apparatus is capable of 12 N of buoyancy force.

The design initially experienced problems with sphericity control. The ceramic balls would tend to decrease in form quality. Removal of convolution in the lower field intensifier and the addition of a water cooling system allowed the polishing apparatus to polish with improving sphericity control.

The analysis of an electromagnetic apparatus with emphasis on comparing results with those found by Umehara et al, has yielded interesting results.

- Higher float forces than those obtained by permanent magnet apparatus, 12 N compared to 7 N
- High material removal with boron carbide abrasive grains, 6 $\mu\text{m}/\text{min}$.
- Low surface roughness with chromium oxide abrasive grains, a minimum of 0.17 μm compared to a minimum of 0.14 μm for Umehara et al
- Decreasing sphericity with time, improving form quality
- Magnetic field variability inside polishing chamber

The design of the original electromagnetic apparatus has been optimized for the polishing process to improve sphericity, reduce surface roughness, and provide an economical method of material removal and ceramic ball element production.

Extensive use of ANSYS finite element package has allowed a number of magnetic apparatus to be conceived, designed, and tested without the necessary labor of actually manufacturing a test apparatus. The final magnetic apparatus design has followed the theoretical ANSYS models closely and results have complied with expectations.

8.2 Recommendations for Future Work

Further work needs to be done on the electromagnetic apparatus to determine its full potential. Varying the shape of the magnetic field intensifier and altering the magnetic field strength and shape may allow higher float forces than previously possible. The sphericity of the ceramic elements might be reduced by improving the stiffness of the magnetic polishing apparatus by increasing the magnetic field gradients inside the polishing chamber or by increasing the stiffness of the bottom float plate with gyroscopic effects.

One method of increasing the stiffness is to drive the lower float plate at higher revolutionary speeds to cause gyroscopic momentum to prevent rapid alterations in the float plate's rotation. This would cause a higher momentary stiffness, but difficulties in construction should be addressed. Driving the lower float plate is difficult because of the position of the float plate inside the polishing chamber, and the position of the driven top plate.

Alterations and improvements to the electromagnetic polishing apparatus will allow the apparatus to be integrated into a production facility for ceramic ball elements, thus lowering the cost of these ball elements to the market. With further advancements economical ball bearings will improve in applicability and expand the capacities of current equipment.

BIBLIOGRAPHY

- Baron, J.M., "Technology of Abrasive Machining in a Magnetic Field," Masino-strojnice, Leningrad (1975) (in Russian)
- Baron, J.M., "Magnetic Abrasive and Magnetic Machining of Machine Parts and Cutting Tools," Leningrad Machine Building, Leningrad, (1986)
- Berkovsky, B.M., Medvedev, V.F., and M.S. Krakov, "Magnetic Fluids," Oxford University Press, (1993) 72
- Childs, T.H.C., Jones, D.A., Mahmood, S., Zhang, B., Kato, K., and N. Umehara, "Magnetic Fluid Grinding Mechanics," *Wear*, 175, (1994) 189-198
- Coats, H.P., "Method and Apparatus for Polishing Containers," US Patent No. 2,196,058 (1940)
- Kurobe, T., "Super Polishing of Ceramic Balls," *Machines and Tools*, (1992)
- Makedonski, B.G. and A.D. Kotschemidov, "Schleifen im Magnetfeld," *Fertigungstechnik und Betrieb*, 24, H.4 (1974) 230-235
- Rosensweig, R.E., "Fluid-magnetic Buoyancy," *AIAA Journal*, 4/10 (1966a) 1751
- Rosensweig, R.E., "Magnetic Fluids," *Int. Sci. Tech.*, (1966b) 48
- Rosensweig, R.E., "A Course in Ferrohydrodynamics," VIII-2 (1980)
- Rosensweig, R.E., U.S. Patent 3,531,413 (1970)
- Shikhirev, B., Matrosov, E., and I. Derech, "Device for Treatment of Sheet Materials," US Patent No. 4,040,209 (1980)
- Shikhirev, B., Matrosov, E., and I. Derech, "Apparatus for Treatment of Sheet Material with the use of Ferromagnetic Powder," US Patent No. 4,187,081 (1980)
- Shikhirev, B., Matrosov, E., and I. Derech, "Apparatus for Working Sheet Materials with Ferromagnetic Powder," US Patent No. 4,204,370 (1980)
- Shinmura, T., Takazawa, K., Hatano, E., and T. Aizawa, "Study on Magnetic -Abrasive Process, Process Principle and Finishing Possibility," *Bull. of JSME*, 19/1, (1985a) 54-55
- Shinmura, T., Takazawa, K., and E. Hatano, "Study on Magnetic-Abrasive Process, Application to Edge Finishing," *Bull. of JSME* 19/3, (1985b) 218-220
- Shinmura, T., Takazawa, K., and E. Hatano, "Advanced Development of Magnetic-Abrasive Finishing and Its Application," *Deburring and Surface Conditioning '85*, Conference Proceedings, Chicago, Illinois, (1985c)
- Shinmura, T., Takazawa, K., and E. Hatano, "Study on Magnetic-Abrasive Finishing, Effects of Machining Fluid on Finishing Characteristics," *Bull. of JSME*, 20/1, (1986a), 52-54

Shinmura, T., Hatano, E., and K. Takazawa, "Development of Spindle-Finish Type Finishing Apparatus and Its Finishing Performace Using a Magnetic Abrasive Machining Process," Bull. of Japan Soc. of Prec. Engg., 20/2, (1986b), 79-84

Shinmura, T., Hatano, E., and K. Takazawa, "The Development of Magnetic-Abrasive Finishing and Its Equipment by Applying a Rotating Magnetic Field," Bull. of JSME, 29/258, (1986c), 4437-4443

Shinmura, T., Takazawa, K., and E. Hatano, "Study on Magnetic Abrasive Finishing, Effects of Various Types of Magnetic Abrasives on Finishing Characteristics," Bull. of Japan Soc. of Prec. Engg., 21/2, (1987), 139-141

Shinmura, T., and T. Aizawa, "Study on Internal Finishing of a Non-ferromagnetic Tubing by Magnetic Abrasive Finishing Process," Bull. of Japan Soc. of Prec. Engg., 23/1, (1989a), 37-41

Shinmura, T., and T. Aizawa, "Study on Magnetic Abrasive Finishing Process," Bull. of Japan Soc. of Prec. Engg., 23/3, (1989b) 236-239

Shinmura, T., Personel Communication (1992)

Tani, Y., and K. Kawata, "Development of High-Efficient Fine Finishing Process Using Magnetic Fluid," Annals of CIRP, 33/1 (1984) 217-220

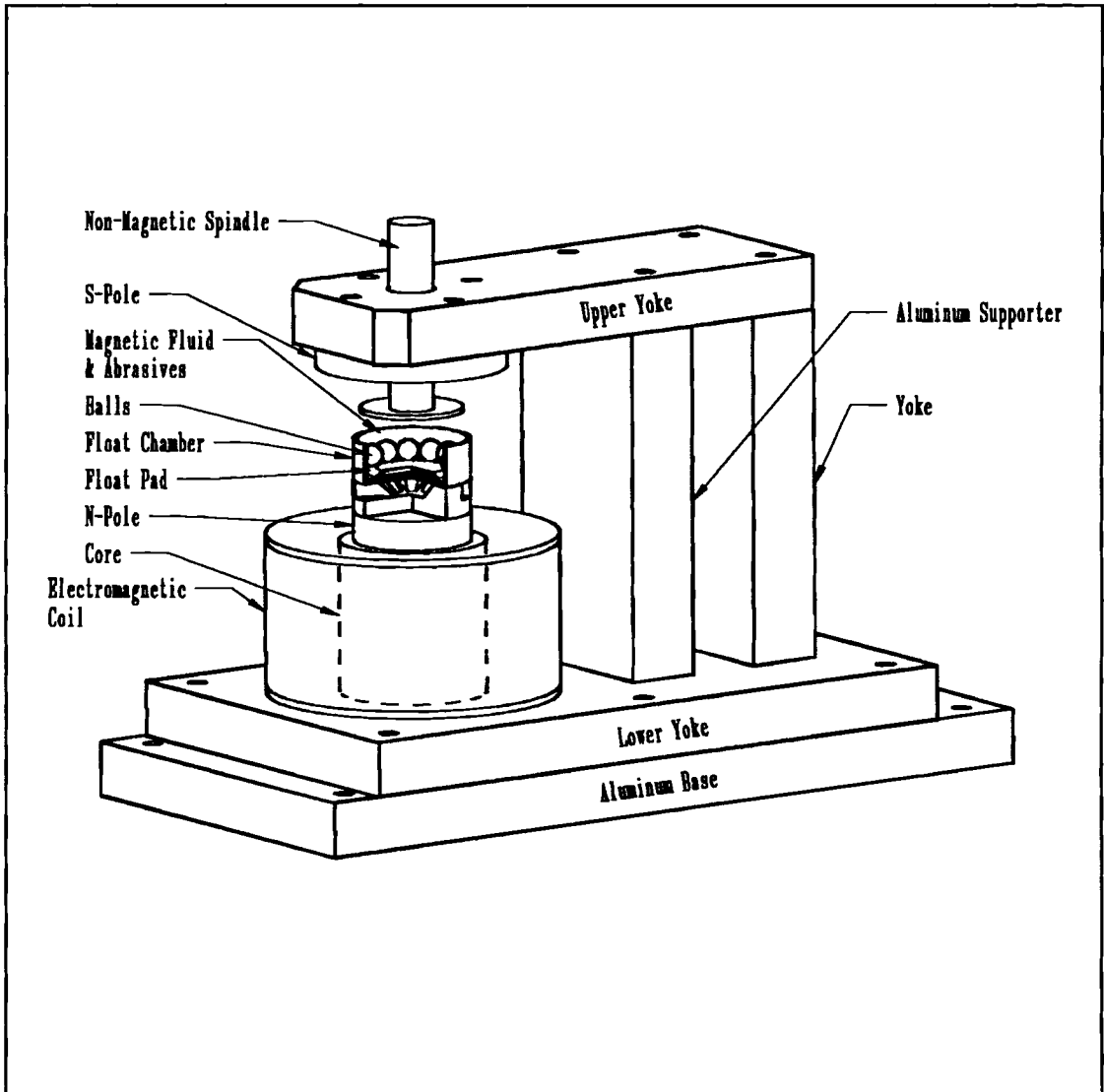
Takazawa, K., Shinmura T., and E. Hatano, "Developemnet of Magnetic Abrasive Finishing and Its Equipment," MR 83-678, Proc. of the SME's 12th Deburring and Surface Conditionoing Conference, Orlando, (Nov 8-10, 1983)

Takazawa, K., Shinmura, T., and E. Hatano, "Advanced Development of Magnetic Abrasive Finishing and Its Equipment," Proc. of the SME's Deburrinig and Surface Conditioning Conference 1985, Orlando, (Sept 23-26, 1985) 30-46

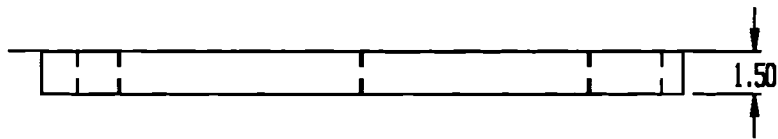
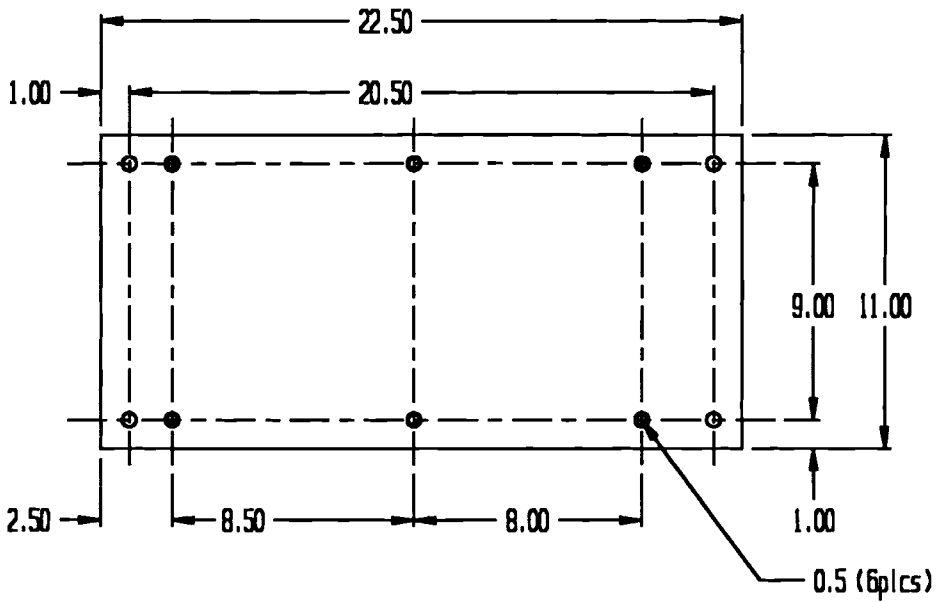
Umehara, N., and K. Kato, "Principles of Magnetic Fluid Grinding of Ceramic Balls," Applied Electromagnetics in Materials, 1, (1990) 37-43

APPENDIX A

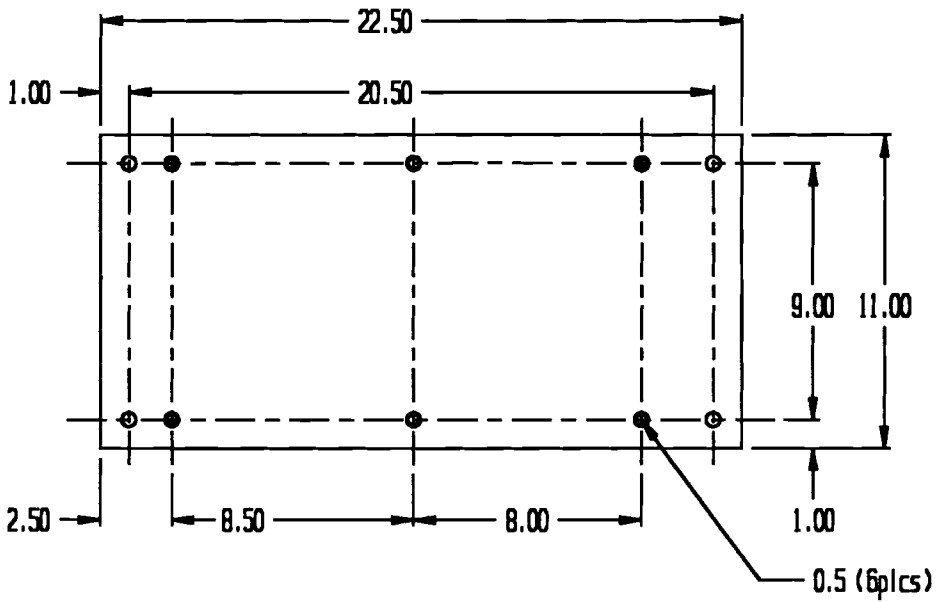
CADKEY DRAWINGS FOR ELECTROMAGNETIC POLISHING APPARATUS



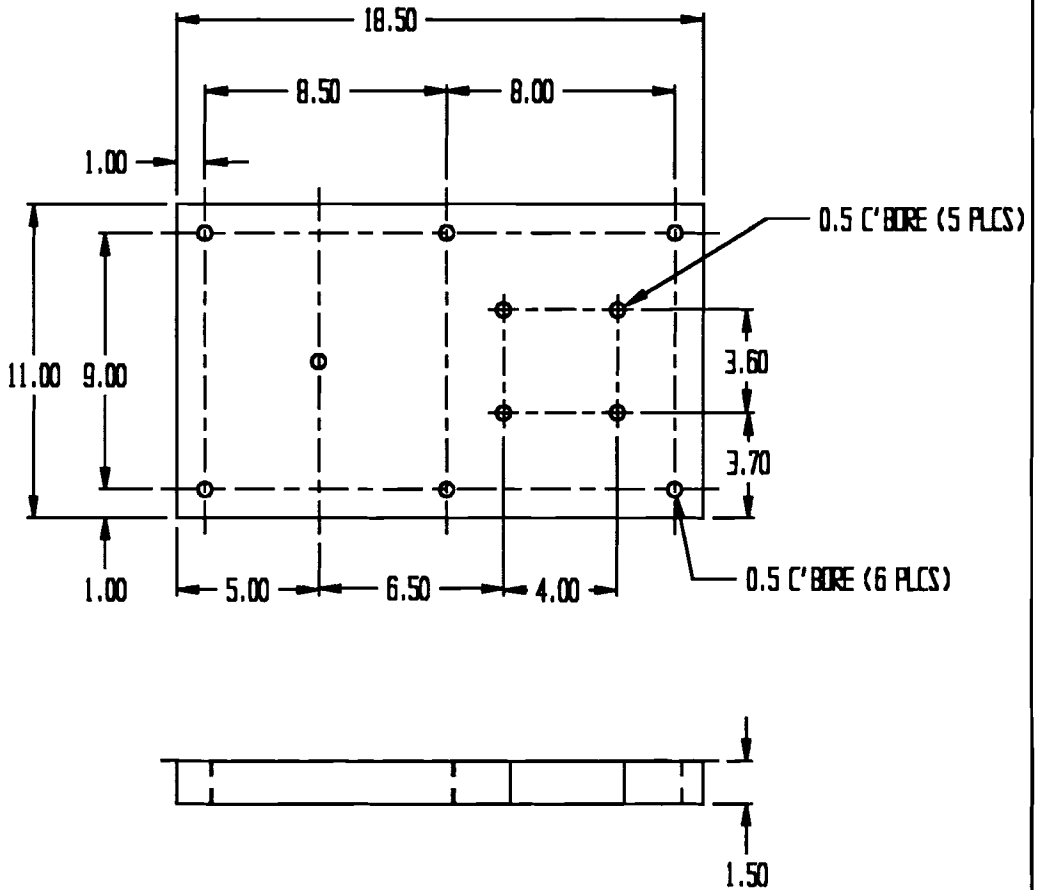
MATERIAL			HEAT TREATMENT		FINISH		QTY
					STILLWATER <i>OSU</i> OKLAHOMA TITLE		
							APPL
			DFT				
REV		DATE	CHK				
USED ON			PART NUMBER				REV



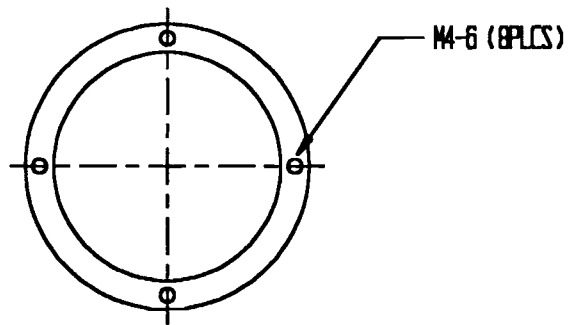
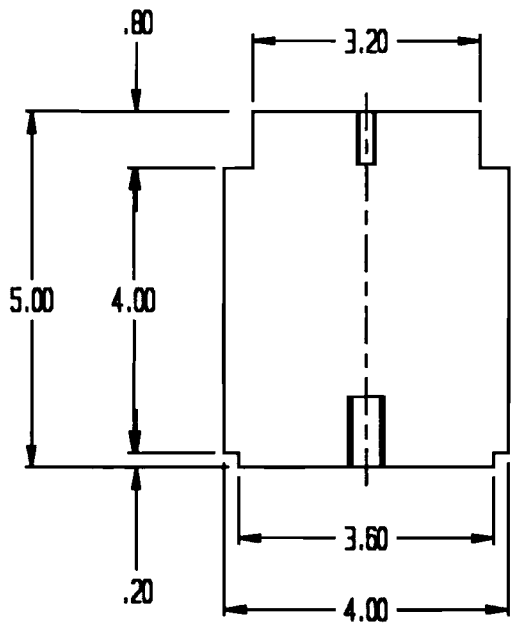
MATERIAL 6061 - T6		HEAT TREATMENT		FINISH	QTY
				STILLWATER <i>OSU</i> OKLAHOMA TITLE Aluminum Base Plate	
REV	DATE	APPL			
		DFT			
		CHK			
USED ON		PART NUMBER			REV



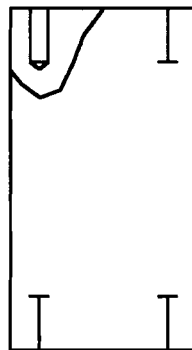
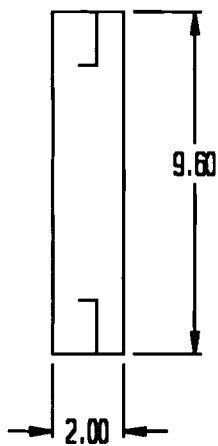
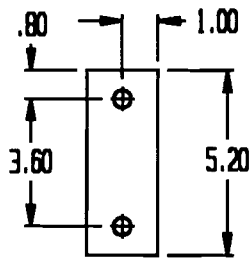
MATERIAL 6061 - T6		HEAT TREATMENT		FINISH		QTY
				STILLWATER <i>OSU</i> OKLAHOMA TITLE Aluminum Base Plate		
						APPL
		DFT				
REV		DATE	CHK			
USED ON			PART NUMBER			REV



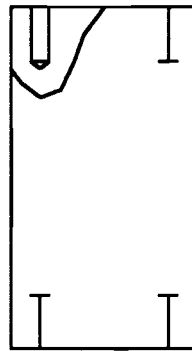
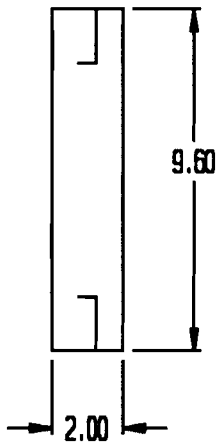
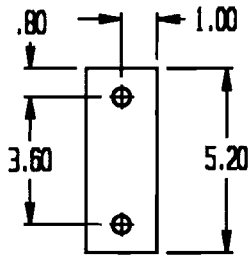
MATERIAL 1018		HEAT TREATMENT		FINISH	QTY
				STILLWATER <i>OSU</i> OKLAHOMA TITLE Steel Base Plate	
		DFT			
REV		DATE	CHK		
USED ON			PART NUMBER		REV



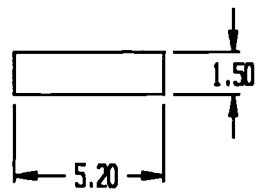
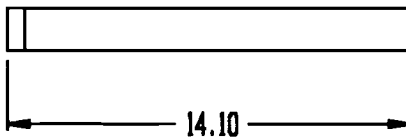
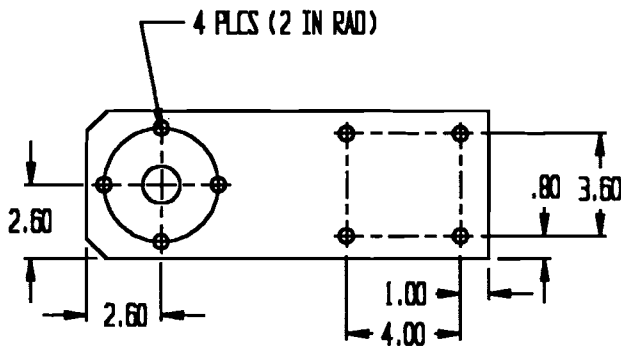
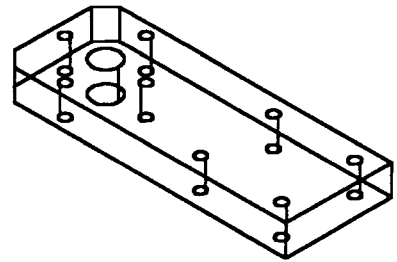
MATERIAL 1018		HEAT TREATMENT		FINISH	QTY
				STILLWATER <i>OSU</i> OKLAHOMA TITLE Magnetic Core	
REV	DATE	APPL			
		DFT			
		CHK			
USED ON		PART NUMBER			REV



MATERIAL 1018		HEAT TREATMENT		FINISH		QTY
				STILLWATER <i>OSU</i> OKLAHOMA TITLE Steel Riser		
REV	DATE	APPL				
		DFT				
		CHK				
USED ON		PART NUMBER				REV



MATERIAL 6061 - T6		HEAT TREATMENT		FINISH	QTY
				STILLWATER <i>OSU</i> OKLAHOMA TITLE Aluminum Riser	
APPL		REV	DATE	CHK	
DFT		PART NUMBER		REV	
USED IN					



MATERIAL 1018		HEAT TREATMENT		FINISH	QTY
				STILLWATER <i>OSU</i> OKLAHOMA TITLE Steel Top Plate	
APPL		REV	DATE	CHK	
DFT		USED ON	PART NUMBER		REV

APPENDIX B

SCRIPT FILES FOR ANSYS MODELING OF ELECTROMAGNETIC FLOAT POLISHING APPARATUS

! Straight Field Geometry Script for ANSYS

/CLEAR

/filnam,str_fld

/prep7

/PNUM,AREA,ON

rectan,-.127,.2,-.019,.019

!Base

RECTAN,-.0457,.0457,.019+.1016,.019+.0203+.1016

!Lower Intensifer

RECTAN,-.0508,.0508,.019,.019+.1016

!Core

AADD,ALL

RECTAN,.0508,.12,.019,.019+.1016

!COIL RIGHT

RECTAN,-.0508,-.12,.019,.019+.1016

!COIL LEFT

RECTAN,.2381,.2,-.019,.26

!RIGHT RISER

RECTAN,.2381,-.1,.26,.26+.0381

!UPPER YOKE

RECTAN,-.1,-.02,.23,.26

!upper intensifier

RECTAN,.02,.1,.23,.26

! " "

AADD,3,6,7,5,4

RECTAN,-.05,.05,.1409,.1409+.05

!FINE AIR POCKET

RECTAN,-.2,.3,-.05,.3

!EXTERNAL AIR

PTXY,-.0254,.1409,-.0152,.1282,.0152,.1282,-.0254,.1409

!CUTOUT

POLY

!RECTAN,.0254,.0457,.1409,.1409+.03

AOVLAP,ALL

AGLUE,ALL

finish

```
!      Straight Field Mesh Script for ANSYS
/prep7
/COM, **** MATERIAL PROPERTY DEFENITION ****
MP, MURX, 1, 1 ! MATL. 1 IS AIR
```

```
TB, BH, 2 ! MATL. 2 IS MILD STEEL
TBPT,,303, 0.8
TBPT,,333.3, 0.9
TBPT,,378.75, 1.0
TBPT,,492.4, 1.1
TBPT,,530.25, 1.2
TBPT,,621.15, 1.3
TBPT,,833.25, 1.33
TBPT,,1000, 1.4
TBPT,,1287.25, 1.45
TBPT,,1666.5, 1.5
TBPT,,2121, 1.55
TBPT,,3000, 1.6
TBPT,,4000, 1.63
TBPT,,5000, 1.645
TBPT,,6000, 1.669
TBPT,,7000, 1.685
TBPT,,8000, 1.7
TBPT,,9000, 1.73
```

```
ET,1,9      !INFINITY
ET,2,13     !FINITE
```

```
asel,all
aclear,all  ! Clear all nodes and elements
lclear,all
```

```
eshape,0
lsel,s,,,31,32 ! select & mesh outer lines
lsel,a,,,24,25
type,1
mat,1
esize,.025
lmesh,all
```

```
asel,s,area,,12 !select & mesh fine air
esla
type,2
mat,1
```

```
ESHAPE,2  
esize,0.001  
amesh,all  
ESHAPE,0
```

```
asel,s,area,,10 !select & mesh fine air  
esla  
type,2  
mat,1  
esize,0.005  
amesh,all  
/wait,10
```

```
asel,s,area,,9 !Select & mesh rough air  
asel,a,area,,6,7  
esla  
type,2  
mat,1  
esize,0.025  
amesh,all
```

```
asel,s,area,,11 !Select & mesh rough steel  
esla  
type,2  
mat,2  
esize,0.025  
amesh,all
```

```
allsel  
save  
finish
```

! Straight Field Solution Script for ANSYS

/solv

ntype,static

nropt,auto

asel,s,area,,9 !select and load left coil

esla

bfe,all,js,3,1.5e6

asel,s,area,,7 !select and load right coil

esla

bfe,all,js,3,-1.5e6

allsel

nsubst,5

kbc,0

neqit,1

lswrite,1

nsubst,1

neqit,20

save

lswrite,2

lssolve,1,2

finish

/post1

save

/show

plnsol,b,y

! Ring Pole Geometry Script for ANSYS

/clear

RINGHGT=0

/filnam,ring_0

/prep7

/PNUM,AREA,ON

rectan,-.127,.127,-.019,.019

!BASE

RECTAN,-.0457,.0457,.019+.1016,.019+.0203+.1016 !Lower Intensifier

RECTAN,-.0508,.0508,.019,.019+.1016 !Core

AADD,ALL

RECTAN,.0508,.12,.019,.019+.1016 !COIL RIGHT

RECTAN,-.0508,-.12,.019,.019+.1016 !COIL LEFT

RECTAN,-.1651,-.127,-.019,.1409+RINGHGT !LEFT RISER

RECTAN,.1651,.127,-.019,.1409+RINGHGT !RIGHT RISER

RECTAN,-.1651,-.05,.1409+RINGHGT,.1409+RINGHGT+.0381 !UPPER LEFT
YOKE

RECTAN,.1651,.05,.1409+RINGHGT,.1409+RINGHGT+.0381 !UPPER RIGHT
YOKE

AADD,3,6,7,5,4

RECTAN,-.05,.05,.1409,.1409+.05 !External Air

RECTAN,-.2,.2,-.05,.25 !EXTERNAL AIR

PTXY,-.0254,.1409,-.0152,.1282,.0152,.1282,.0254,.1409 !CUTOUT

POLY

AOVLAP,ALL

aadd,15,17,18,19

AGLUE,ALL

finish

```

!      Ring Pole Meshing Script for ANSYS
/prep7
/COM, **** MATERIAL PROPERTY DEFENITION ****
MP, MURX, 1, 1 ! MATL. 1 IS AIR
TB, BH, 2 ! MATL. 2 IS MILD STEEL
TBPT,,303, 0.8
TBPT,,333.3, 0.9
TBPT,,378.75, 1.0
TBPT,,492.4, 1.1
TBPT,,530.25, 1.2
TBPT,,621.15, 1.3
TBPT,,833.25, 1.33
TBPT,,1000, 1.4
TBPT,,1287.25, 1.45
TBPT,,1666.5, 1.5
TBPT,,2121, 1.55
TBPT,,3000, 1.6
TBPT,,4000, 1.63
TBPT,,5000, 1.645
TBPT,,6000, 1.669
TBPT,,7000, 1.685
TBPT,,8000, 1.7
TBPT,,9000, 1.73

ET,1,9      !INFINITY
ET,2,13     !FINITE

asel,all
aclear,all  ! Clear all nodes and elements
lclear,all

eshape,0
lsel,s,,,23,25,1 ! select & mesh outer lines
lsel,a,,,27
type,1
mat,1
esize,.025
lmesh,all

asel,s,area,,12 !select & mesh fine air
asel,a,area,,14 !select & mesh fine air
esla
type,2
mat,1
esize,0.005

```

amesh,all
/wait,10

asel,s,area,,7 !Select & mesh rough air
asel,a,area,,9,11,1
asel,a,area,,6
esla
type,2
mat,1
esize,0.025
amesh,all

asel,s,area,,13 !Select & mesh rough steel
esla
type,2
mat,2
esize,0.025
amesh,all

allsel
save
finish

```
!      Ring Pole Solution Script for ANSYS
```

```
/solv
```

```
ntype,static
```

```
nropt,auto
```

```
asel,s,area,,11      !select and load left coil
```

```
esla
```

```
bfe,all,js,3,1.5e6
```

```
asel,s,area,,10      !select and load right coil
```

```
esla
```

```
bfe,all,js,3,-1.5e6
```

```
allsel
```

```
nsubst,5
```

```
kbc,0
```

```
neqit,1
```

```
lswrite,1
```

```
nsubst,1
```

```
neqit,20
```

```
save
```

```
lswrite,2
```

```
lssolve,1,2
```

```
finish
```

```
/post1
```

```
/show
```

```
plnsol,b,y
```

APPENDIX C

PROGRAM UTILIZED FOR DETERMINATION OF BUOYANT FORCES

```

/*****
*
*   Program for Determination
*   of Magnetic Float Forces
*
*   by   Matthew Dock
*
*****/
#include <stdio.h>
#define FerroM 600
float mag(float);

void main()
{
int n,i,j=1,k=0, sign, num;
float
x[140],y[140],node[140],Bx[140],By[140],val,Bfld[10][14],Xfld[10][14],Yfld[10][14];
float Fb,A,H,dH, mu,PI=3.1416;
char fname[20],strn[20];
FILE *fp;
mu= 4*PI*1e-7;

printf("\n Pl. give input file name : ");
scanf("%s", fname);
fp = fopen(fname,"r");
if(fp==NULL)
{
printf("file not found\n");
exit(i);
}
for(i=0;i<7;i++)
{
j=0;
while(j==0)
{
fscanf(fp,"%s",strn);
if((strncmp(strn,"THZX",5)==0))
{
for(k=0;k<20;k++)
{
fscanf(fp,"%f%f%f%f%f%f%f",
&node[i*20+k],&x[i*20+k],
&y[i*20+k],&val,&val,&val,&val);
printf("%f\n",node[i*20+k]);
}
}
}
}

```

```

        j=1;
        }
    }
}

for(i=0;i<3;i++)
{
    j=0;
    while(j==0)
    {
        fscanf(fp,"%s",strn);
        if((strcmp(strn,"BSUM",5)==0))
        {
            for(k=0;k<37;k++)
            {
                fscanf(fp,"%f%f%f%f%f",
                    &node[i*37+k],&Bx[i*37+k],
                    &By[i*37+k],&val,&val);
            }
            j=1;
        }
    }
}

j=0;
while(j==0)
{
    fscanf(fp,"%s",strn);
    if((strcmp(strn,"BSUM",5)==0))
    {
        for(k=0;k<29;k++)
        {
            fscanf(fp,"%f%f%f%f%f",
                &node[3*37+k],&Bx[3*37+k],
                &By[3*37+k],&val,&val);
        }
        j=1;
    }
}

fclose(fp);
for(i=0;i<10;i++)
for(j=0;j<14;j++)
{
    Bfld[i][j]=By[i*14+j];
    Xfld[i][j]=x[i*14+j]-.027245+.003;
}

```

```

    }
    printf("          Y          Fb\n");
    for(j=0;j<12;j++)
    {
        Fb=0;
        for(i=9;i>j;i--)
        {
            H=(Bfld[i][j])/mu;
            dH=(H-Bfld[i][j+1])/mu;
            A=((Xfld[i][j])*(Xfld[i][j])-(Xfld[i-1][j])*(Xfld[i-1][j]))*PI;
            Fb=mag(H)*dH*A*mu+Fb;
        }
        printf("%4.4e          %4.4e\n",y[j],Fb);
    }
}

```

```

float mag(float H)
{
    if(H>100000)
        return((47747));
    else
        return(FerroM*H/100000*1000/(4*3.1416));
}

```

VITA

Matthew Dock

Candidate for the Degree of

Master of Science

Thesis: ELECTROMAGNETIC FLOAT POLISHING OF
CERAMIC BALLS FOR BEARING
APPLICATIONS

Major Field: Mechanical Engineering

Biographical:

Personal Data: Born in Tulsa, Oklahoma, On July 16, 1970, the son of
Marshall and Patsy Dock.

Education: Graduated from Sand Springs High School, Sand Springs,
Oklahoma in May 1988; received Bachelor of Science degree in
Mechanical Engineering from Oklahoma State University,
Stillwater, Oklahoma in May 1992. Completed the requirements
for the Master of Science degree with a major in Mechanical
Engineering at Oklahoma State Univeristy in May 1995.

Experience: Worked as chemistry laboratory technician at Oklahoma
State Univeristy while attending freshman year; worked as resi
dent assistant for residential life at Oklahoma State University; 1
year of cooperative education with Hilti Inc., from Tulsa,
Oklahoma; employed by Oklahoma State University for ceramic
bearing research program during Master of Science study.